

# NAVAL POSTGRADUATE SCHOOL

## Monterey, California



## THESIS

**ERROR ANALYSIS OF REAL-TIME REMOTELY SENSED  
MICROWAVE SEA-ICE MOTIONS IN THE WESTERN  
ARCTIC OCEAN**

by

David M. Carsten

September 2000

Thesis Advisor:  
Second Reader:

Philip A. Durkee  
Jeffrey L. Haferman

Approved for public release; distribution is unlimited.

DTIC QUALITY INSPECTED 4

20010215 075

<b>REPORT DOCUMENTATION PAGE</b>			Form Approved OMB No. 0704-0188	
Public reporting burden for this collection of information is estimated to average 1 hour per response, including the time for reviewing instruction, searching existing data sources, gathering and maintaining the data needed, and completing and reviewing the collection of information. Send comments regarding this burden estimate or any other aspect of this collection of information, including suggestions for reducing this burden, to Washington headquarters Services, Directorate for Information Operations and Reports, 1215 Jefferson Davis Highway, Suite 1204, Arlington, VA 22202-4302, and to the Office of Management and Budget, Paperwork Reduction Project (0704-0188) Washington DC 20503.				
<b>1. AGENCY USE ONLY (Leave blank)</b>		<b>2. REPORT DATE</b> September 2000	<b>3. REPORT TYPE AND DATES COVERED</b> Master's Thesis	
<b>4. TITLE AND SUBTITLE:</b> ERROR ANALYSIS OF REAL-TIME EMOTELY SENSED MICROWAVE SEA-ICE MOTIONS IN THE EASTERN ARCTIC OCEAN			<b>5. FUNDING NUMBERS</b>	
<b>6. AUTHOR(S)</b> David M. Carsten				
<b>7. PERFORMING ORGANIZATION NAME(S) AND ADDRESS(ES)</b> Naval Postgraduate School Monterey, CA 93943-5000			<b>8. PERFORMING ORGANIZATION REPORT NUMBER</b>	
<b>9. SPONSORING / MONITORING AGENCY NAME(S) AND ADDRESS(ES)</b> N/A			<b>10. SPONSORING / MONITORING AGENCY REPORT NUMBER</b>	
<b>11. SUPPLEMENTARY NOTES</b> The views expressed in this thesis are those of the author and do not reflect the official policy or position of the Department of Defense or the U.S. Government.				
<b>12a. DISTRIBUTION / AVAILABILITY STATEMENT</b> Approved for public release; distribution is unlimited			<b>12b. DISTRIBUTION CODE</b>	
<b>13. ABSTRACT (maximum 200 words)</b>  An algorithm used to composite SSM/I 85.5 GHz imagery and derive sea ice motion was adapted for operational testing at Fleet Numerical Meteorology and Oceanography Command (FNMOC). A feature tracking technique was applied to a 6-month period, with data provided by FNMOC and the Naval Research Laboratory (NRL). Ice motions are detectable using the SSM/I motion algorithm, and fields of SSM/I motion vectors are qualitatively consistent with coincident fields of in situ buoy motion vectors. Accuracy of the SSM/I motion vectors relative to buoy motion vectors increase significantly with buoy speed. No correlation between SSM/I and buoy motion vectors is observed for speeds below 3 cm/s and correlation increases significantly above 5 cm/s. The results are very sensitive to compositing techniques used to combine SSM/I passes into a single sea ice representation. FNMOC data was composited using a "drop-in-the-bucket" technique while NRL data was composited by a bi-linear interpolation technique. Significantly poorer results were found with FNMOC composited data.				
<b>14. SUBJECT TERMS</b>  Special Sensor Microwave/Imager (SSM/I), Microwave, 85.5 GHz, sea ice motion, ice motion algorithm, in-situ buoy data, summary statistics, correlation			<b>15. NUMBER OF PAGES</b>	
			<b>16. PRICE CODE</b>	
<b>17. SECURITY CLASSIFICATION OF REPORT</b>  Unclassified	<b>18. SECURITY CLASSIFICATION OF THIS PAGE</b>  Unclassified	<b>19. SECURITY CLASSIFICATION OF ABSTRACT</b>  Unclassified	<b>20. LIMITATION OF ABSTRACT</b>  UL	

THIS PAGE INTENTIONALLY LEFT BLANK

Approved for public release; distribution is unlimited.

**ERROR ANALYSIS OF REAL-TIME REMOTELY SENSED MICROWAVE  
SEA-ICE MOTIONS IN THE WESTERN ARCTIC OCEAN**

David M. Carsten  
Lieutenant Commander, United States Navy  
B.S., Oregon State University, 1990

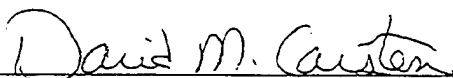
Submitted in partial fulfillment of the  
requirements for the degree of

**MASTER OF SCIENCE IN METEOROLOGY  
AND PHYSICAL OCEANOGRAPHY**

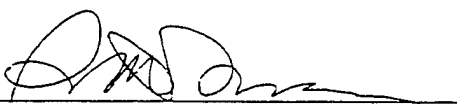
from the

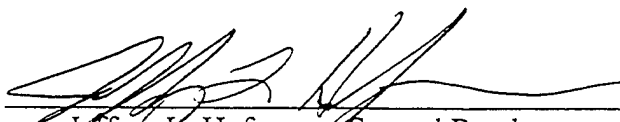
**NAVAL POSTGRADUATE SCHOOL  
September 2000**

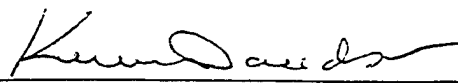
Author:

  
David M. Carsten

Approved by:

  
Philip A. Durkee, Thesis Advisor

  
Jeffrey L. Haferman, Second Reader

  
For Robert L. Haney, Chairman  
Department of Meteorology

THIS PAGE INTENTIONALLY LEFT BLANK

## ABSTRACT

An algorithm used to composite SSM/I 85.5 GHz imagery and derive sea ice motion was adapted for operational testing at Fleet Numerical Meteorology and Oceanography Command (FNMOC). A feature tracking technique was applied to a 6-month period, with data provided by FNMOC and the Naval Research Laboratory (NRL). Ice motions are detectable using the SSM/I motion algorithm, and fields of SSM/I motion vectors are qualitatively consistent with coincident fields of in situ buoy motion vectors. Accuracy of the SSM/I motion vectors relative to buoy motion vectors increase significantly with buoy speed. No correlation between SSM/I and buoy motion vectors is observed for speeds below 3 cm/s and correlation increases significantly above 5 cm/s. The results are very sensitive to compositing techniques used to combine SSM/I passes into a single sea ice representation. FNMOC data was composited using a "drop-in-the-bucket" technique while NRL data was composited by a bi-linear interpolation technique. Significantly poorer results were found with FNMOC composited data.

THIS PAGE INTENTIONALLY LEFT BLANK

## TABLE OF CONTENTS

VI.	INTRODUCTION.....	1
A.	MOTIVATION .....	2
B.	OBJECTIVES .....	3
II.	THEORY .....	5
A.	MEASUREMENTS .....	5
B.	RADIATIVE TRANSFER .....	5
C.	THE 85.5 GHZ SENSOR .....	7
III.	DATA .....	9
A.	INSTRUMENTS .....	9
1.	Special Sensor Microwave/Imager (SSM/I) .....	9
2.	Arctic Buoys .....	10
B.	DATA SETS .....	13
1.	FNMOC SSM/I Data .....	13
2.	Naval Research Laboratory (NRL) SSM/I Data .....	13
3.	International Arctic Buoy Programme (IABP) .....	13
4.	NOGAPS .....	14
IV.	PROCEDURE .....	15
A.	OVERVIEW .....	15
B.	METHODOLOGY .....	15
1.	Synoptic Situation.....	15
2.	Ice Motion Algorithm.....	16
3.	Ice Motions .....	17
4.	SSM/I/Buoy Vector Matching .....	21
V.	RESULTS AND DISCUSSION .....	25
A.	CASE STUDY DISCUSSION .....	25
1.	Case Study 1: December 27 - 29 <sup>th</sup> , 1999 (SSM/I from NRL) .....	25
2.	Case Study 2: January 15 - 16th, 2000 (SSM/I from NRL) .....	37
3.	Case Study 3: February 17 - 18th, 2000 (SSM/I data from NRL and FNMOC).....	46
4.	Case Study 4: March 06 - 08th, 2000 (SSM/I from FNMOC) .....	54
B.	SUMMARY STATISTICS.....	59
C.	NRL/FNMOC STATISTICAL SUMMARY FOR MAY 11-14 <sup>TH</sup> .....	69
D.	VECTOR CORRELATION .....	73
VI.	CONCLUSIONS AND RECOMMENDATIONS.....	77
A.	CONCLUSIONS .....	77
B.	RECOMMENDATIONS.....	78
VII.	LIST OF REFERNCES.....	81
VIII	INITIAL DISTRIBUTION LIST .....	83



THIS PAGE INTENTIONALLY LEFT BLANK

## LIST OF FIGURES

Figure 1. Frequency/Wavelength Spectrum. ....	6
Figure 2. Orbital characteristics of the DMSP Satellite and 85.5 GHz channel. ....	10
Figure 3. An ICEX-AIR buoy capsule. ....	11
Figure 4(a-d). 4a is a composited 12.5 km resolution satellite image containing 608x896 $T_B$ pixels. 4b is a standard ice motion vector plot at every 10 $T_B$ pixels. A 5 $T_B$ pixel overlap in 4c computes ice motion vectors every 62.5 km. 4d reflects oversampling a $T_B$ pixel at 1/4 increment, computing ice motion every 3.1 km or 3.62 cm/s. ....	18
Figure 5. SSM/I 85.5GHz motion vector image using IDL. ....	21
Figure 6. Closest SSM/I/Buoy match grid cell dimensions. ....	22
Figure 7. Median SSM/I/Buoy match grid cell dimensions. ....	23
Figure 8. Plotted SSM/I and buoy motion vectors for December 27, 28 and 29 <sup>th</sup> , 1999 at 1200Z. ....	29
Figure 9. Closest and median SSM/I motion vector match using a 0.7 correlation for ..... December 27 <sup>th</sup> , 1999 at 1200Z. ....	30
Figure 10. Median SSM/I motion vector match using a 0.7 and 0.9 correlation for ..... December 27 <sup>th</sup> , 1999 at 1200Z. ....	31
Figure 11. Closest and Median SSM/I motion vector match using a 0.7 correlation for ..... December 28 <sup>th</sup> , 1999 at 1200Z. ....	32
Figure 12. Median SSM/I motion vector match using a 0.7 and 0.9 correlation for ..... December 28 <sup>th</sup> , 1999 at 1200Z. ....	33
Figure 13. Highlighted area of closest SSM/I and buoy motion vector plot ..... using a 0.7 correlation (L.H.S.). Area 1 zoomed (R.H.S.) for ..... December 28 <sup>th</sup> , 1999 at 1200Z. ....	34
Figure 14. Closest and median SSM/I motion vector match using a 0.7 correlation for ..... December 29 <sup>th</sup> , 1999 at 1200Z. ....	35
Figure 15. Median SSM/I motion vector match using a 0.7 and 0.9 correlation for ..... December 29 <sup>th</sup> , 1999 at 1200Z. ....	36
Figure 16. Plotted SSM/I and buoy motion vectors for January 15 <sup>th</sup> , at 1200Z and ..... January 16 <sup>th</sup> , 2000 at 0000Z and 1200Z. ....	39
Figure 17. Closest and median SSM/I motion vector match using a 0.7 correlation for ..... January 15 <sup>th</sup> , 2000 at 1200Z. ....	40
Figure 18. Median SSM/I motion vector match using a 0.7 and 0.9 correlation for ..... January 15 <sup>th</sup> , 2000 at 1200Z. ....	41
Figure 19. Closest and median SSM/I motion vector match using a 0.7 correlation for ..... January 16 <sup>th</sup> , 2000 at 0000Z. ....	42
Figure 20. Median SSM/I motion vector match using a 0.7 and 0.9 correlation for ..... January 16 <sup>th</sup> , 2000 at 0000Z. ....	43
Figure 21. Closest and median SSM/I motion vector match using a 0.7 correlation for ..... January 16 <sup>th</sup> , 2000 at 1200Z. ....	44
Figure 22. Median SSM/I motion vector match using a 0.7 and 0.9 correlation for ..... January 16 <sup>th</sup> , 2000 at 1200Z. ....	45

Figure 23. Plotted SSM/I and buoy motion vectors for February 18 <sup>th</sup> , 2000 at 0000Z ..... (NRL and FNMOC SSM/I Data).....	49
Figure 24. Plotted SSM/I and buoy motion vectors for February 18 <sup>th</sup> , 2000 at 1200Z ..... (NRL and FNMOC SSM/I Data).....	50
Figure 25. Closest SSM/I motion vector match using a 0.7 correlation for ..... February 18 <sup>th</sup> , 2000 at 0000Z (NRL and FNMOC SSM/I Data).....	51
Figure 26. Median SSM/I motion vector match using a 0.7 correlation for ..... February 18 <sup>th</sup> , 2000 at 0000Z (NRL and FNMOC SSM/I Data).....	52
Figure 27. Median SSM/I motion vector match using a 0.9 correlation for ..... February 18 <sup>th</sup> , 2000 at 0000Z (NRL and FNMOC SSM/I Data).....	53
Figure 28. Plotted SSM/I and buoy motion vectors for March 06 - 08th, 2000 at 1200Z.... (FNMOC SSM/I Data).....	56
Figure 29. Closest and median SSM/I motion vector match using a 0.7 correlation for ..... March 07th, 2000 at 1200Z (FNMOC SSM/I Data).....	57
Figure 30. Median SSM/I motion vector match using 0.7 and 0.9 correlation for ..... March 07th, 2000 at 1200Z (FNMOC SSM/I Data).....	58
Figure 31. Polar plot using a 0.7 correlation threshold (NRL data) December 01, 1999 to February 29, 2000. ....	65
Figure 32. Polar plot using a 0.9 correlation threshold (NRL data) ..... December 01, 1999 to February 29, 2000.....	66
Figure 33. Polar plot using a 0.9 correlation threshold on (FNMOC data) ..... February 15 to May 30, 2000.....	67
Figure 34. Polar plot using a 0.9 correlation threshold on (FNMOC data) ..... February 15 to May 30, 2000.....	68
Figure 35. FNMOC Polar plot using a 0.7 correlation threshold..... May 11 - 14 <sup>th</sup> , 2000.....	71
Figure 36. FNMOC Polar plot using a 0.7 correlation threshold..... May 11 - 14 <sup>th</sup> , 2000.....	72
Figure 37. Vector correlation coefficient ( $R^2$ ) plot of 0.7 correlated threshold.....	74
Figure 38. Vector correlation coefficient ( $R^2$ ) plot of 0.9 correlated threshold.....	75

## LIST OF TABLES

Table 1. SSM/I channel characteristics.....	7
Table 2. Buoy characteristics (May 1 <sup>st</sup> , 2000).....	12
Table 3. Example data file from IABP .....	14
Table 4. Selected case studies .....	16
Table 5. Normalized Speed and Relative Direction statistics for the 0.7 correlation threshold December 01, 1999 to February 29, 2000. (NRL data) .....	60
Table 6. Normalized Speed and Relative Direction statistics for the 0.9 correlation threshold December 01, 1999 to February 29, 2000. (NRL data) .....	61
Table 7. Normalized Speed and Relative Direction statistics for the 0.7 correlation threshold December 01, 1999 to February 29, 2000. (FNMOC data). .....	62
Table 8. Normalized Speed and Relative Direction statistics for the 0.9 correlation threshold December 01, 1999 to February 29, 2000. (FNMOC data) .....	63
Table 9. Normalized Speed and Relative Direction statistics for the 0.7 correlation threshold, May 11 - 14 <sup>th</sup> , 2000 (FNMOC data). .....	70
Table 10. Normalized Speed and Relative Direction statistics for the 0.7 correlation threshold, May 11 - 14 <sup>th</sup> , 2000 (NRL data).....	70

THIS PAGE INTENTIONALLY LEFT BLANK

## ACKNOWLEDGMENTS

I would like to thank my advisor, Dr. Philip A. Durkee, Department of Meteorology and Mr. Jeff Haferman of Fleet Numerical Meteorology and Oceanography Center, for their professional guidance and support during the development of this thesis. I owe debts of gratitude to Mr. Kurt Nielsen of the Remote Sensing Laboratory (RSL) and Mr. Robert Creasey of the Naval Postgraduate School's Interactive Digital Environmental Analysis (IDEA) Laboratory. Kurt and Bob provided extensive support in computer programming, software application and UNIX operating system. Without their assistance, I would have been extremely pressed to complete my analysis.

My sincere appreciation to Mr. Joe Turk of the Naval Research Laboratory, and the science team of Mr. Ignatius Rigor and Mr. Mark Ortmeyer at the Polar Science Center, Applied Physics Lab, University of Washington, for their buoy data contributions used in this study.

Mr. Don Stark of the Naval Postgraduate School, LT Sean Memmen and Dr. Walt Meier of the National Ice Center are also to be thanked for providing support throughout my endeavor.

Finally, a special loving thanks to my wife Becky, son Nathan, and daughters Jennifer and Holly, whose patience and love throughout this effort inspired me to maintain focus on what truly is important in life, my family.

THIS PAGE INTENTIONALLY LEFT BLANK

## I. INTRODUCTION

Passive microwave observations of polar oceans have become essential to the tracking of ice motions, estimating sea ice concentrations, and for classifying sea ice types. Ice formation and movement has always been a concern to Naval, DOD and commercial shipping. Global ice information, immediately practical for use in shipping and petroleum development activities, has broader implications for the meteorological foundations of modeling climate change.

Remotely sensed microwave imagery provides an excellent data source for computation of sea ice motions. Resulting ice motions can further be assimilated into polar ice prediction models used by the National Ice Center (NIC) and Fleet Numerical Meteorology and Oceanography Center (FNMOC).

Buoys set in Arctic ice provide a continuous, although spatially limited source of ice motion information. Buoy positions are accurate to within 350 meters (Colony and Thorndike 1984). Though sparse and unevenly distributed, they are useful in evaluating the quality of SSM/I derived ice motions. The scarcity of in-situ buoy observations leads to the importance of using satellite-based SSM/I analysis to derive ice motion.



## **A. MOTIVATION**

Previous studies of derived SSM/I ice motion have centered on using archived data. Temporal periods have ranged from 24 and 72-hour derived ice motions, to monthly and multi-year climatic studies (Emery et al. 1991, Emery et al., 1997, Kwok et al., 1998). Traditionally, ice motions are derived for the entire Arctic basin. Computing daily SSM/I ice motions will provide FNMOC and NIC real-time ice motions that are useful for application in daily ice motion products and various modeling programs.

Knowledge of the location and extent of sea ice has always been of vital importance. Assimilating sea ice motions into polar ice prediction models would certainly produce better operational ice motion products. Our only direct method of obtaining surface meteorological parameters in the Arctic comes from a limited number of buoys spread throughout the Arctic Ocean. They provide highly accurate temporal and spatial data, though very sparse in spatial coverage. Ice motions produced on a synoptic scale will provide useful input for future ice motion product development at NIC and modeling development for the U.S. Navy's Polar Ice Prediction System (PIPS 3.0) model. Incorporating daily SSM/I sea ice motion data should greatly enhance accuracies of these products.

Ice motions in this study are derived from passive microwave imagery acquired by the Special Sensor Microwave/Imager (SSM/I) aboard the Defense Meteorological Satellite Program (DMSP) satellites F-11/13/14/15 (F-11 was turned off Spring 2000). The microwave spectrum is used as clouds are mostly transparent and ice has a higher emittance than water, making it detectable using the Microwave Imager. Data acquired

by the Advanced Very High Resolution Radiometer (AVHRR) has a much higher resolution, but visible and infrared radiation is not transparent to clouds. Data acquired by the Synthetic Aperture Radar (SAR) is limited by spatial coverage and very large files that cause time acquisition constraints that prevent the day-to-day operational use required by FNMOC and NIC. The DMSP SSM/I program is designed to provide a continuous flow of data, which FNMOC assimilation techniques require for their models.

## **B. OBJECTIVES**

The object of this paper is to perform a quantitative and qualitative assessment of ice motions derived from an ice motion algorithm developed by Meier (1999). Case studies are developed to analyze SSM/I derived ice motions and compare them to in-situ Arctic buoy motions. Normalized SSM/I and buoy speed differences, and relative differences in SSM/I and buoy direction are computed on a daily timeframe. The correlation of buoy and SSM/I motion vectors provide a quantitative evaluation of the ice motion algorithm and the value of SSM/I derived vectors. To be useful for this purpose, SSM/I derived motions will be analyzed daily. Our goal is to imitate FNMOC's daily routine of receiving the raw SSM/I data, processing it through the ice motion algorithm, and making derived ice motions available for assimilation into polar prediction models. By imitating FNMOC procedures, we can provide a quality assessment that is useful to determine any algorithm characteristics that may require updating for future application.

Resulting correlations will provide FNMOC and NIC a tool from which to assess SSM/I derived ice motion accuracy and aid in assignment of a quality parameter, used for assimilating parameters into polar models.

THIS PAGE INTENTIONALLY LEFT BLANK

## **II. THEORY**

### **A. MEASUREMENTS**

Satellite multi-channel passive microwave sensors provide global radiance measurements from which to map, monitor and study Arctic sea ice motion. The SSM/I microwave radiometer measures the emitted energy from the earth and atmosphere in the microwave frequency spectrum. The seven frequencies (in GHz) and polarizations of the SSM/I are 19.3 V (vertical polarization), 19.3 H (horizontal polarization), 22.235 V, 37.0 V, 37.0 H, 85.5 V, and 85.5 H. For sea ice motions, the 85.5 GHz horizontally polarized channel is used, since the spatial resolution (12.5 km) of this channel and its sensitivity to ice properties provides the best opportunity to compute ice motions.

### **B. RADIATIVE TRANSFER**

Radiative transfer theory provides the basis for methods used to determine sea-ice motion from remote sensing. In the microwave part of the EM spectrum we typically work with frequency ( $\nu$ ) rather than wavelength ( $\lambda$ ) as the spectral variable. The 85.5 GHz frequency is located in a region of high transmittance relative to lower surrounding water vapor and oxygen transmittance bands. Figure 1 shows an annual mean transmittance value of 0.8 at 85.5 GHz for 15° north latitude. Transmittance is typically greater at polar latitudes due to reduced water vapor within the atmosphere.

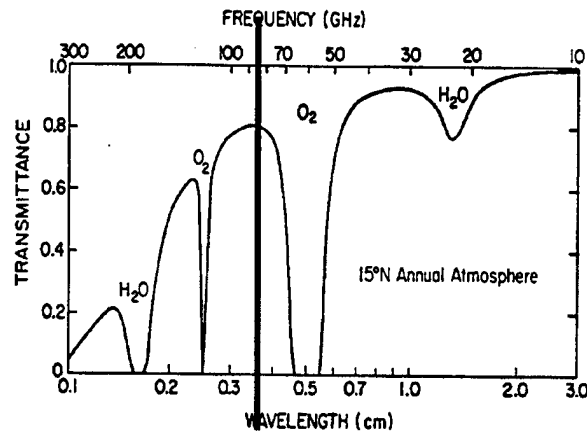


Figure 1. Frequency/Wavelength Spectrum.

Frequencies are small enough (or wavelengths long enough) so that the *Planck function* can be simplified into a linear function referred to as *Rayleigh-Jeans Approximation* (Kidder and Vonder Haar, 1995). Temperatures encountered on the earth and atmosphere at centimeter and millimeter wavelengths can be estimated. Since the *Rayleigh-Jeans Approximation* holds in the microwave wavelength regime, the emitted energy is proportional to the temperature of the radiator.

The emission characteristics of the passive microwave signature of sea ice are a function of electromagnetic properties of the surface and surface temperature. The brightness temperature when transmittance is equal to 1.0 is defined as  $T_B = \epsilon T_s$ , where  $\epsilon$  is the emissivity and  $T_s$  is the physical surface temperature. Emissivity is the fraction of radiant energy that a perfect black body would emit at the same physical temperature, dependent upon the electromagnetic (EM) properties of the emitting surface, frequency and polarization.

The emitted microwave radiance is sensitive to the emission characteristics of open water, first-year ice and multi-year ice. Water is highly reflective in the microwave range and characterized by strong differences between horizontal and vertical

polarization. Emission values of water for the 85.5GHz channel are 0.79 for vertical polarization and 0.53 for horizontal polarization (Meier 1998) and therefore appear radiatively cold. First year ice has an emissivity value of around 0.9. The higher value makes the ice appear radiatively warmer than open water and therefore detectable in contrast to water. The emissive value of multi-year ice is variable as properties of old ice are complex and its structure varies. The typical value is found to be around 0.7 and therefore appears radiatively cooler than first year ice. Complications in interpreting microwave signatures occur during the spring and summer months as the 85.5 GHz channel is susceptible to atmospheric water vapor and emissive properties of melt ponds that collect on the ice surface. This gives the ice a lower emissive value, therefore appearing radiatively cold as in open water.

### C. THE 85.5 GHZ SENSOR

A particular advantage of using microwave frequencies is the insensitivity to solar irradiance, clouds and other atmospheric effects that inhibit visible and infrared frequencies. The 85.5 GHz microwave frequency sensor is used for ice motion detection as it provides better resolution required in determining small ice motions normally found in the Arctic. Table 1 provides SSM/I sensor characteristics for all channels.

**Table 1. SSM/I channel characteristics**

$\nu$ (GHz)	$\lambda$ (cm)	Resolution
85.5	0.35	12.5 km
37.0	0.81	25.0 km
22.235	1.36	25.0 km
19.3	1.58	25.0 km

Calculation of ice motions using microwave imagery does not require detection and detailed analysis of ice characteristics. The only requirement is that ice features dominate the variations of brightness temperature in a given image. Detection of the movement of these features in successive images can then be confidently ascribed to ice motion.

### **III. DATA**

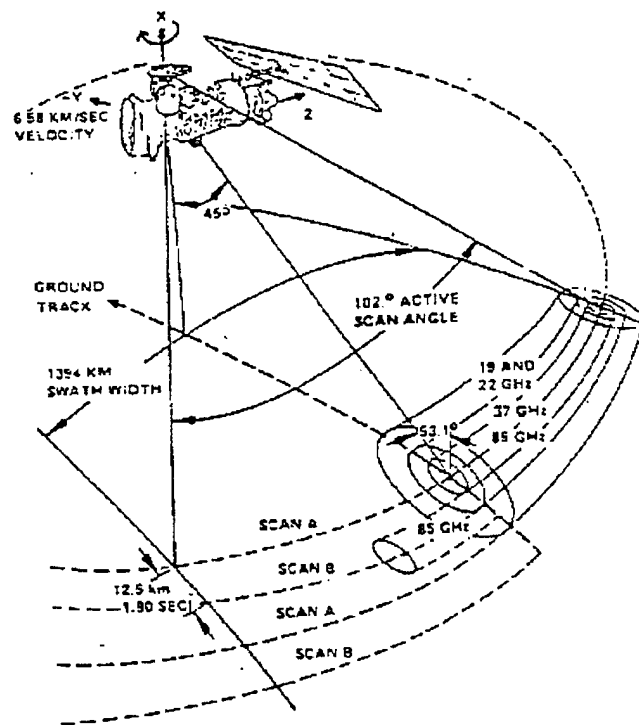
To validate the SSM/I ice-motion algorithm for the real time application described in this thesis, data sets were selected based on the availability of in-situ buoy measurements and receipt of near real time satellite data. Composited satellite images with resulting ice motion vectors were matched to buoy observations both in space and time. This chapter will describe the data sets and instrumentation used to collect the data used in this study.

#### **A. INSTRUMENTS**

##### **1. Special Sensor Microwave/Imager (SSM/I)**

The SSM/I is a seven-channel, four-frequency, linearly polarized, passive microwave radiometric system that measures scene microwave brightness temperatures at 19.35, 22.235, 37.0, and 85.5 GHz (Table 1.). SSM/I is carried aboard Defense Meteorological Satellite Program (DMSP) satellites, F11, F13, F14 and F15. They maintain an altitude of approximately 830km in a polar orbit. DMSP satellites provide excellent polar coverage, as the orbital period is approximately 102 minutes. This is especially beneficial for microwave imaging of sea ice, as numerous passes will provide a dataset that covers the polar region in a little over 12 hours.





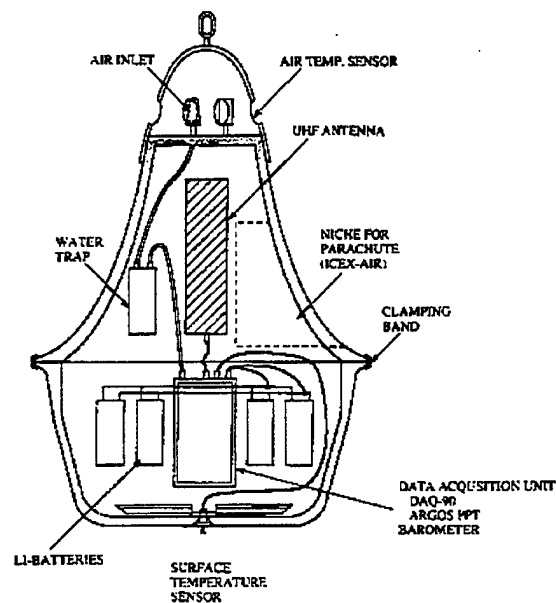
**Figure 2.** Orbital characteristics of the DMSP Satellite and 85.5 GHz channel.

Figure 2 shows swath data characteristics of the SSM/I imager (PODAAC, 2000). A swath consists of A/B scan pairs, which include 256 radiance measurements. Large circles signify all SSM/I microwave channels, while the small circles signify the 85.5 GHz channel. The 85.5 GHz channel provides double the information than other channels and at better resolution. A constant  $45.4^\circ$  angle of view measures the upwelling scene brightness temperatures allowing wind effects to be detectable on the surface.

## 2. Arctic Buoys

The International Arctic buoy Programme (IABP) is located in the Polar Science Center, Applied Physics Laboratory, at the University of Washington. They maintain a network of automated data buoys in the Arctic Basin that monitor synoptic-scale fields of pressure, temperature, and ice motion that provide real-time support to Arctic operations

and meteorological and oceanographic research. Table 2 provides a listing of buoys tracked by the IABP. A total of 28 different buoys were used for this study, most of which were ICEX-AIR buoys. Figure 3 provides an example of the ICEX-AIR Arctic buoy that provided Meteorological and motion parameters used in this study. Detailed buoy diagrams are located on the IABP web page (IABP 1996).



**Figure 3.** An ICEX-AIR buoy capsule.

**Table 2. Buoy characteristics (May 1<sup>st</sup>, 2000)**

DATE	ARGOS	WMO	EXPR	GTS	Latitude	Longitude	Data	Pres	Temp	Buoy
DEPLOYED	ID	ID	NUMBER	HEADER			Bytes			Description
Aug 1999	1222	48601	484	SSVX01-LFPW	78.247	-178.728	17	Y	Y	ICEX-AIR
Aug 1996	1261	48102	484	SSVX01-LFPW	76.823	-177.884	17			ICEX-AIR
Apr 1998	1301	48581	1053	SSVX02-CWEG	83.496	-79.899	16	Y	Y	Met ocean
Aug 1998	1351	48532	484	SSVX01-LFPW	79.474	-144.666	17	Y	Y	ICEX-AIR
Aug 1998	1793	48533	29	SSVX01-LFPW	76.287	-150.107	17	Y	Y	ICEX-AIR
Aug 1998	1905	25525	557	SSVX12-KARS	78.106	147.28	21	Y	Y	ICEX-AIR
Aug 1998	1906	25526	557	SSVX12-KARS	80.566	172.59	21	Y	Y	ICEX-AIR
Apr 2000			557	SSVX12-KARS	89.486	107.518	4	Y	Y	JAMSTEC
Sep 1998	2388	25557	1053	SSVX12-KARS	78.754	-157.273	32	Y		CES
Mar 2000	2415	48579	1053	SSVX02-CWEG	79.691	-131.255	32	Y	Y	CES
Apr 1998	2416	47523	1053	SSVX02-CWEG	75.084	-138.695	32	Y		ZENO-3200
Sep 1997	2417	48572	1053	SSVX02-CWEG	79.202	-146.843	16	Y		CES
Mar 2000	2418	48577	1053	SSVX02-CWEG	77.646	-133.176	32	Y	Y	CES
Aug 1998	3004	25535	1053	SSVX12-KARS	81.29	154.186	17	Y	Y	ICEX-AIR
Aug 1999	3311	25569	919	SSVX01-LFPW	82.444	162.32	21	Y	Y	ICEX-AIR
Aug 1999	3691	25012	314	SSVX01-LFPW	77.241	175.92	21	Y	Y	ICEX-AIR
Apr 1998	4954	48580	1053	SSVX02-CWEG	75.622	-139.509	32	Y		ZENO-3200
Apr 2000	5300		627	SSVX02-CWEG	89.58	-107.301	4	Y	Y	CALIB
Aug 1999	5312	48523	627	SSVX02-CWEG	75.518	-176.566	17	Y	Y	ICEX-AIR
Mar 1999	5313	47538	627	SSVX02-CWEG	78.94	-120.64	16	Y	Y	ICEX-AIR
Mar 2000	5317	48524	627	SSVX02-CWEG	84.803	-116.723	24	Y	Y	EC
Mar 2000	5318	48525	627	SSVX02-CWEG	81.47	-111.34	24	Y	Y	EC
Apr 2000	7091	26509	282	SSVX16-KARS	89.351	-12.784	2	Y	Y	NAVO
Apr 2000	7092	26510	282	SSVX16-KARS	88	161.688	12	Y	Y	NAVO
Apr 2000	8059	71541	919	SSVX01-LFPW	88.804	-91.473	23	Y	Y	AWI
Aug 1999	8065	25570	919	SSVX01-LFPW	77.015	163.65	21	Y	Y	ICEX-AIR
Apr 2000	8066	71547	919	SSVX01-LFPW	87.35	-92.609	23	Y	Y	AWI
May 1992	10667	48531	1016	SSVX02-CWEG	71.672	170.519	32	Y	Y	IOEB
Aug 1996	19578	47602	1053	SSVX12-KARS	75.725	-126.329	16			ICEX-AIR
Apr 2000	20726	695			89.49	-105.661	32			PMEL
Aug 1999	20858	48574	1053	SSVX12-KARS	76.062	-176.6	17	Y	Y	ICEX-AIR
Aug 1999	20859	48575	1053	SSVX12-KARS	77.009	-166.904	17	Y	Y	ICEX-AIR
Apr 2000	22203		695		89.497	-105.525	4			PMEL
Sep 1997	22204		695		80.146	-154.58	32			PMEL
Apr 2000	22206		695		89.488	-105.332	32			PMEL
Apr 2000	22207		695		89.522	-107.314	32			PMEL
Sep 1997	26696	48576	1053	SSVX12-KARS	79.606	-156.326	32	Y	Y	CES
Jul 1996	26699	48573	1053	SSVX02-CWEG	84.381	-96.966	32			CES

## **B. DATA SETS**

### **1. FNMOC SSM/I Data**

Fleet Numerical provided daily SSM/I files from February 15<sup>th</sup> through May 30<sup>th</sup>, 2000. A minimum number of case studies were selected for analysis and comparison. Exceptionally large SSM/I data files and composited imagery prohibited the storage of 6-months worth of data. A subjective process was used to isolate periods of Meteorological conditions that the author deemed important for application of Meier's algorithm.

### **2. Naval Research Laboratory (NRL) SSM/I Data**

The premise of this paper was to study a 6-month period of ice-motions. FNMOC data only covered February – May, so NRL provided SSM/I data in TeraScan data format from December 1<sup>st</sup>, 1999 through February 29<sup>th</sup>, 2000. This provided an overlap where both FNMOC and NRL data were available for 15-29 February. NRL and FNMOC apply different geolocation and antenna correction patterns to their SSM/I data sets. Therefore, the differences in ice-motion results derived from the two data sets were examined during the overlap period. Also, compositing NRL SSM/I data was accomplished using a routine in TeraScan. A February case study is examined to determine if compositing differences occur and result in different SSM/I motion vectors.

### **3. International Arctic Buoy Programme (IABP)**

Arctic buoy data was made available on a monthly basis from IABP. Table 3 depicts typical buoy data characteristics. This study uses buoy U and V wind

components, and latitude and longitude coordinates for purposes of plotting and deriving buoy motion vectors.

**Table 3. Example data file from IABP**

Buoy number	Year	Julian day	GMT	Latitude	Longitude	SLP (mb)	Air-Temp °C	U (cm/s)	V (cm/s)
14955	1999	335	0	85.8052	-169.878	1017	-18.3	0.8287	-5.4236
14955	1999	335	12	85.8028	-169.388	1017	-17.6	1.2372	-11.224
14955	1999	336	0	85.7984	-168.681	1017	-16.6	1.2094	-9.9548
14955	1999	336	12	85.7971	-168.325	1019	-16.7	1.0648	-6.9224

#### **4. NOGAPS**

The Naval Operational Global Atmospheric Prediction System (NOGAPS) Meteorological fields provided a data set of surface temperature, sea-level pressure in millibars (mbs) and 10-meter winds at one-degree resolution. NOGAPS fields were used as a ground truth to check motions provided by buoy observations and compare directional SSM/I vectors against expected motions resulting from a given synoptic wind pattern.

## **IV. PROCEDURE**

### **A. OVERVIEW**

SSM/I ice motion fields are expected to be most accurate during winter, when surface and atmospheric conditions are optimum for tracking. The SSM/I derived motion fields are most valuable for representing large-scale, persistent patterns of sea ice transport. Consecutive 85.5 GHz SSM/I imagery provide comprehensive estimates of sea ice motion on a uniform grid for sea ice covered areas of the Arctic. The scale resolution is not adequate for comparison of fine-scale motions over shorter time intervals, but is suited for investigating coarser-scale patterns and processes affected by synoptic-scale weather events.

### **B. METHODOLOGY**

#### **1. Synoptic Situation**

Long-term climatic studies of ice motion fields using ice-tracking algorithms applied to the 85.5 GHz microwave imagery have produced results representative of the general Arctic circulation pattern (Emery et al., 1997). This thesis used daily 14-hour composites to derive ice motions on a time-scale reflective of FNMOC's daily operating procedures. Meteorological synoptic mean sea level pressure, 10-meter winds, and buoy locations were plotted simultaneously with the ice motion analysis. The cases cover periods of different meteorological conditions throughout the six-month period. A list of Case studies is provided in Table 4.

**Table 4. Selected case studies**

Case Studies		
	Date	Synoptic Situation
Case 1	December 27 - 29 <sup>th</sup> 1999	Low Pressure transits western Arctic with High Pressure and increasing pressure gradient.
Case 2	January 15 - 16 <sup>th</sup> 2000	Low Pressure transits western Arctic with distinctive wind shift north of Nome AK and increasing pressure gradient.
Case 3	February 17 - 18 <sup>th</sup> 2000	Light pressure gradient as Arctic High Pressure ridge extends from west to east.
Case 4	March 06 - 08 <sup>th</sup> 2000	Intensifying Arctic High Pressure with a strong constant pressure gradient.

## **2. Ice Motion Algorithm**

The ice motion algorithm for 85.5 GHz SSM/I imagery presented here was developed by Chuck Fowler and Bill Emery at the university of Colorado (Fowler 1995; Emery et al. 1997) and adapted by Meier (1999) for integration at FNMOC. Deriving sea ice motions from a 24hr, 72hr or monthly satellite composite may mask the algorithm's ability to depict short-term changes. The 14-hour period used here was selected to ensure complete geographical satellite coverage of the Arctic Ocean and provide the highest possible time resolution.

The microwave imager can detect change in the varying ice characteristics by detecting the change in brightness temperature ( $T_B$ ) features in a target area. The basic approach involves comparing two spatially consecutive composite images 12 or 24 hours apart and searching for the similar  $T_B$  patterns in each image (Meier 1999). The

displacement of a  $T_B$  pattern between images is determined and a motion vector is calculated.

A contiguous matrix of  $10 \times 10$   $T_B$  target areas would produce an ice displacement calculation every  $T_B$  pixel (12.5km) and plots one motion vector every 10  $T_B$  pixels (125km). A routine within the algorithm allows the user to overlap a portion of the  $T_B$  matrix. An overlap of 5  $T_B$  pixels was chosen, resulting in ice motion vectors being plotted every 5  $T_B$  pixels (62.5 km).

Another routine of the ice motion algorithm allows over sampling the array to calculate motion. Over sampling moves the target area in 1/4-pixel increments. This allows detection of  $T_B$  features to be correlated and ice motion to be derived at a displacement resolution of 3.1 km or speed resolution of 3.62 cm/s.

### **3. Ice Motions**

Four steps are required to produce ice motions from FNMOC SSM/I raw data files.

- a. Routines within the algorithm are used to convert raw SSM/I files obtained from FNMOC into brightness temperatures. This is a two-step process where the data is first converted to antenna temperature ( $T_A$ ) and then converted into brightness temperatures ( $T_B$ ).



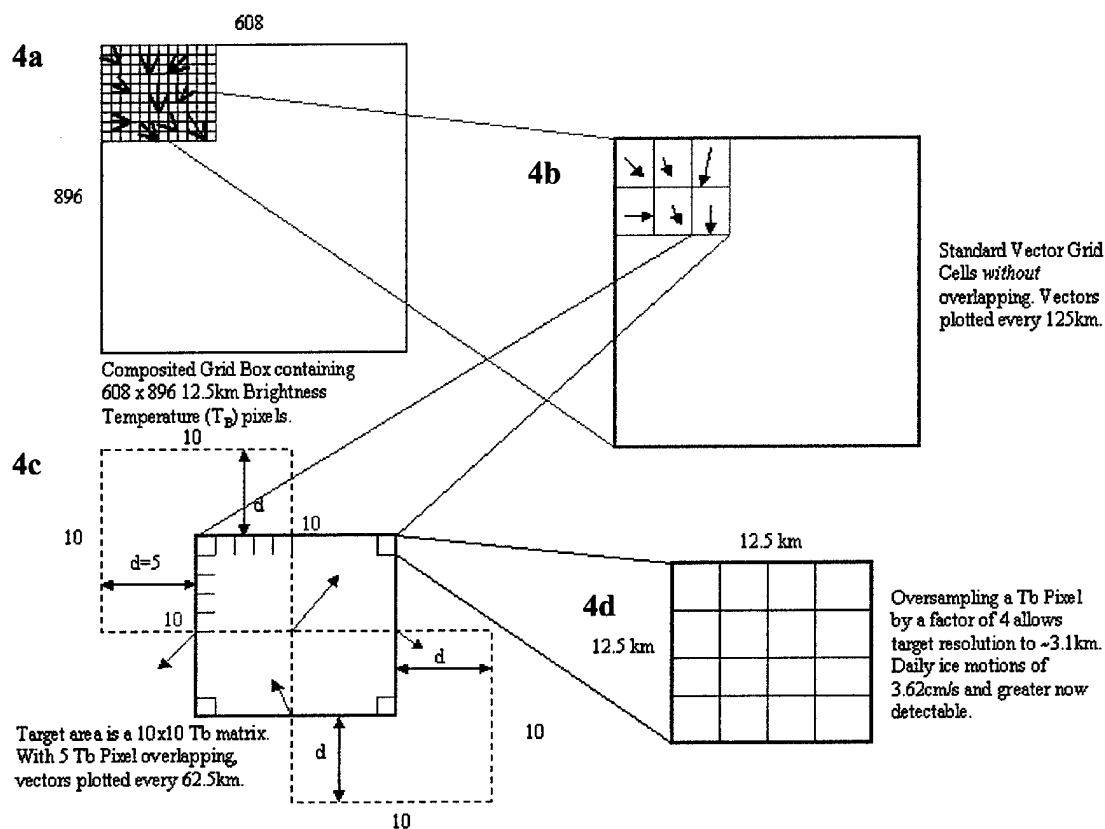


**Figure 4(a-d).** 4a is a composited 12.5 km resolution satellite image containing 608x896  $T_B$  pixels. 4b is a standard ice motion vector plot at every 10  $T_B$  pixels. A 5  $T_B$  pixel overlap in 4c computes ice motion vectors every 62.5 km. 4d reflects over sampling a  $T_B$  pixel at 1/4 increment, computing ice motion every 3.1 km or 3.62 cm/s.

b. Figure 4(a) reflects a composite that consists of a 608 x 896 grid of Brightness Temperature ( $T_B$ ) pixels. Brightness temperatures are composited and gridded onto the NSDIC polar stereographic grid (NSDIC 1997). Interactive Data Language (IDL) procedures are used for compositing and mapping. The 85.5 GHz horizontal polarization channel is extracted from the  $T_B$  files, composited and gridded. The IDL sub-procedure *mapll.pro* was modified as part of this analysis to correct the gridding routines.

As earlier stated, a 14-hour composite is used for this study. The algorithm bins  $T_B$  values using the drop-in-the-bucket method ( $T_B$  pixel values are binned from individual SSM/I passes and averaged). A 6-hour, 12-hour and 24-hour composite was investigated. A 6-hour composite left several open gaps in coverage. A 12-hour composite often left a small section of the Arctic with incomplete coverage. A 24-hour composite increases temporal averaging, which could lead to smoothing and excessive binning of brightness temperatures, which skew actual motion results. The 14-hour composite provided complete coverage of the Arctic and was chosen to reflect FNMOC's 12-hour watch routine and reduce motion uncertainties that result from smoothing.

c. Once composite images are created, a motion field is calculated. The algorithm performs an automated method of calculating ice motion. A feature match between images is determined by the maximum correlation (minimum difference) of  $T_B$  pixel values in a 10x10 pixel target area. The maximum cross correlation (MCC) of the target area provides an objective method for computing ice motion from consecutive composited images. Correlations of a target area in the first image are compared to all regions in a pre-set search area in the second image.

Figure 4(b) is a standard ice motion vector plot at every 10  $T_B$  pixels. The highest correlated peak (MCC method) within the target search area is located and an ice motion derived. One ice motion vector is plotted every 125 km or 14.42 cm/s. Figure 4(c) shows the 5  $T_B$  pixel overlap used for this study. This allows the computation of ice motion vectors every 62.5 km or 7.23 cm/s. Figure 4(d) shows the effect of over sampling. The target area is sampled in 1/4  $T_B$  pixel increments, computing ice motion at a spatial displacement of 3.1 km or speed resolution of 3.62 cm/s.

Filtering of motion vectors is applied in order to delete erroneous motions. A pre-set correlation threshold value of 0.7 in the algorithm's filter routine was initially used for this study. Correlation is a measure of the match between consecutive target area arrays. Any matching feature that produced an ice motion vector in a target area between images that correlated below 0.7 will be filtered and not plotted.

In theory, a correlation threshold value of 0.9 has a higher risk of filtering good motion vectors, just as a 0.7 correlation threshold risks inclusion of a higher number of bad vectors. This thesis examines the effect of the correlation filter. Motion vector fields were generated with values of 0.7 and 0.9 and the results will be discussed in Chapter V.

d. The filtered motion file is plotted using an IDL routine. Figure 5 shows an example of plotted motions using this routine. To conduct a comparison analysis between FNMOC and NRL SSM/I data with in-situ buoy motions, the ASCII file of motion vectors were plotted with TeraScan.



**Figure 5.** SSM/I 85.5GHz motion vector image using IDL.

## **2. SSM/I/Buoy Vector Matching**

Two methods were used in this study to compare SSM/I motion vectors with buoy motion vectors. First, the closest SSM/I vector within a specified  $T_B$  pixel grid radius was selected and matched to a co-located buoy. Figure 6 shows the closest SSM/I vector in a target area, matched to a buoy. . In theory, one SSM/I vector will always be located within a  $2.5 T_B$  pixel radius (31.25 km) centered on the buoy. The correlation threshold of 0.7 or 0.9 will remove many ice motion vectors, resulting in SSM/I vector motion gaps. This often leaves a buoy unmatched with an SSM/I motion vector.

Selecting the closest SSM/I motion vector does not always provide an adequate qualitative assessment of the actual SSM/I motion vector field. Correlated motion vectors are often erroneous or sparse, leaving no match for a buoy. The second method expands the  $T_B$  pixel radius to include more than one SSM/I ice motion vector. Figure 7 shows a 5  $T_B$  pixel radius or 62.5 km. Extending our radius enables up to 5 SSM/I ice motion vectors to be located near, and centered on a buoy. The median value of the SSM/I motion vectors is then matched to its corresponding buoy. As with method one, the SSM/I ice motion vectors must meet the assigned correlation threshold.

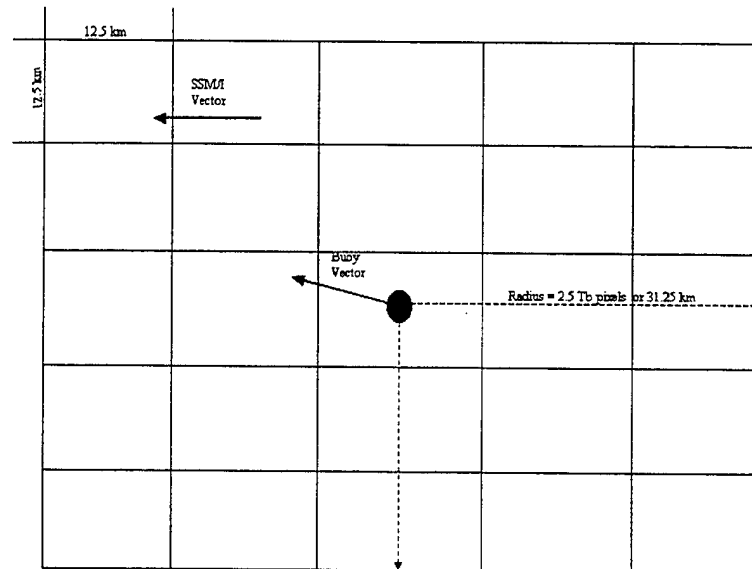


**Figure 6.** Closest SSM/I/Buoy match grid cell dimensions.

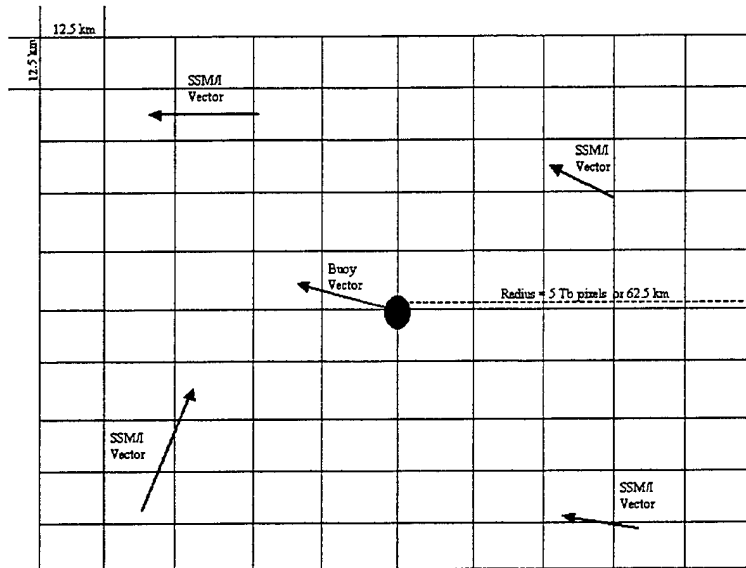


**Figure 7.** Median SSM/I/Buoy match grid cell dimensions.

THIS PAGE INTENTIONALLY LEFT BLANK

## **V. RESULTS AND DISCUSSION**

### **A. CASE STUDY DISCUSSION**

The following case studies display full coverage SSM/I and buoy motion vector fields. The effects of varying the correlation threshold between 0.7 and 0.9, and differences between matching a buoy to its nearest SSM/I motion vector and to the median of neighboring SSM/I vectors, are described.

#### **1. Case Study 1: December 27 - 29<sup>th</sup>, 1999 (SSM/I from NRL)**

Figure 8 is a full coverage plot of SSM/I and buoy motion vectors for the period of December 27 - 29<sup>th</sup>, 1999 at 1200Z. A definite synoptic change is reflected as surface winds increase in response to a strengthening pressure gradient. SSM/I and buoy motion vector magnitudes substantially increase in response to the increased wind speeds. .

Figure 9 is a SSM/I and buoy motion vector match comparison plot using a 0.7 correlation threshold for December 27<sup>th</sup>, 1999 at 1200Z. The left-hand plot matches the closest SSM/I motion vector, with the right-hand plot matching the median SSM/I motion vector to its corresponding buoy. SSM/I and buoy motion vector pairs increase as a result of using the median SSM/I motion vector. Overall, SSM/I speed and direction values are better reflective of buoy values using the median SSM/I vector.

Figure 10 is a SSM/I and buoy motion vector match comparison plot using a 0.7 and 0.9 correlation threshold for December 27<sup>th</sup>, 1999 at 1200Z. Overall, SSM/I speed and direction values with 0.9 correlation threshold better reflect buoy values. One good



SSM/I and buoy match using 0.7 correlation threshold was eliminated with the 0.9 correlation threshold.

Figure 11 is a SSM/I and buoy motion vector match comparison plot for the closest and median matching techniques using a 0.7 correlation threshold for December 28<sup>th</sup>, 1999 at 1200Z. The closest SSM/I motion vector match does better on this day. The median SSM/I vector set creates more pairs and SSM/I speed and direction values are distinctly more reflective of buoy values.

Figure 12 is a plot of SSM/I and buoy motion vector pairs comparing a 0.7 and 0.9 correlation threshold for December 28<sup>th</sup>, 1999 at 1200Z. Results are similar to December 27<sup>th</sup> in that SSM/I motion vectors with a 0.9 correlation filter agree with buoy vector values better than a 0.7 correlation. Two good SSM/I and buoy vector pairs using 0.7 correlation threshold are eliminated with the 0.9 correlation threshold.

Figure 13 is a SSM/I and buoy motion vector field image for December 28<sup>th</sup>, 1999 at 1200Z. The closest neighboring SSM/I motion vector in the left-hand image is selected and highlighted by 'Zoom area 1'.  $T_B$  grid cells are visibly detectable on the right-hand image and reveal that the only SSM/I vector within a  $2.5 T_B$  pixels radius (31.25 km) from its matching buoy has an erroneous vector speed of 29 cm/s and an erroneous direction. Lower in the image, the buoy with a motion of 7 cm/s appears to be surrounded by accurate SSM/I motion vectors. In this example, the closest SSM/I to buoy match approach fails to include information from good vectors surrounding the buoy (see Fig. 6).

Referring back to Figure 11, the median SSM/I motion vector method depicts several new SSM/I and buoy motion vector pairs. Expanding the  $T_B$  pixel radius to 5

(62.5km) and computing an SSM/I median, allows the opportunity to include good vectors in our analysis (see Fig. 7).

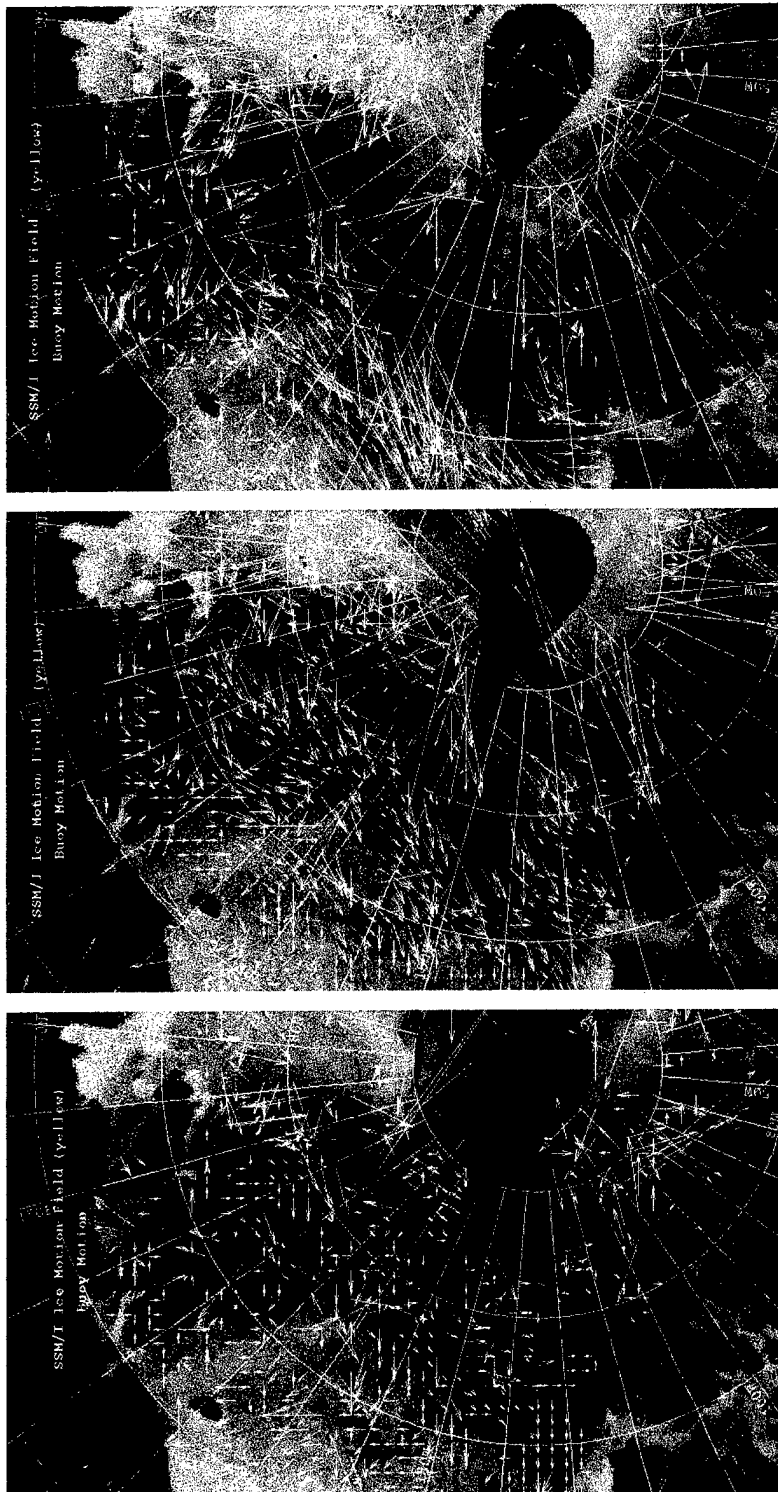
Figure 14 is a SSM/I and buoy motion vector match comparison plot using a 0.7 correlation threshold for December 29<sup>th</sup>, 1999 at 1200Z. The synoptic pattern and high surface winds are clearly reflected in the SSM/I and buoy motion vectors. The median SSM/I vector match clearly adds value, as more pairs are displayed and earlier SSM/I speed and direction values are more reflective of buoy values. Two matched pairs are clearly erroneous, but they passed the 0.7 correlation threshold filter and are plotted.

Figure 15 is a SSM/I and buoy motion vector match comparison plot using a 0.7 and 0.9 correlation threshold for December 29<sup>th</sup>, 1999 at 1200Z. The 0.9 correlation threshold removes one of the erroneous pairs and results in more agreement between SSM/I and buoy values for two pairs of vectors. Two good SSM/I and buoy pairs are removed.

***Summary for Case study 1 (NRL SSM/I data):*** The December 27 - 29<sup>th</sup> time period was selected to identify differences in resulting SSM/I motion vectors by applying different methods of SSM/I motion vector selections, and by varying the correlation threshold. This time period starts with buoy motions of 3-6 cm/s that increase to 10-26 cm/s in response to an increasing surface pressure gradient.

Case 1 provided insightful information concerning the SSM/I motion vector selection process. Selection of the closest SSM/I motion vector to the corresponding buoy resulted in a small number of buoy pairs, and often paired the buoy with an erroneous SSM/I vector. Applying a median to SSM/I motion vectors within a  $T_B$  radius provided better results. Several more SSM/I and buoy motion vector pairs

were selected and the qualitative comparisons suggest improvement in their agreement. Correlation thresholds of 0.7 and 0.9 mirrored one another as both provided excellent SSM/I and buoy motion vector pairs. The 0.9 correlations tended to remove good and bad vector pairs, but overall provided slightly better values when compared to the 0.7 correlation threshold.



**Figure 8.** Plotted SSM/I and buoy motion vectors for December 27, 28 and 29<sup>th</sup>, 1999 at 1200Z.

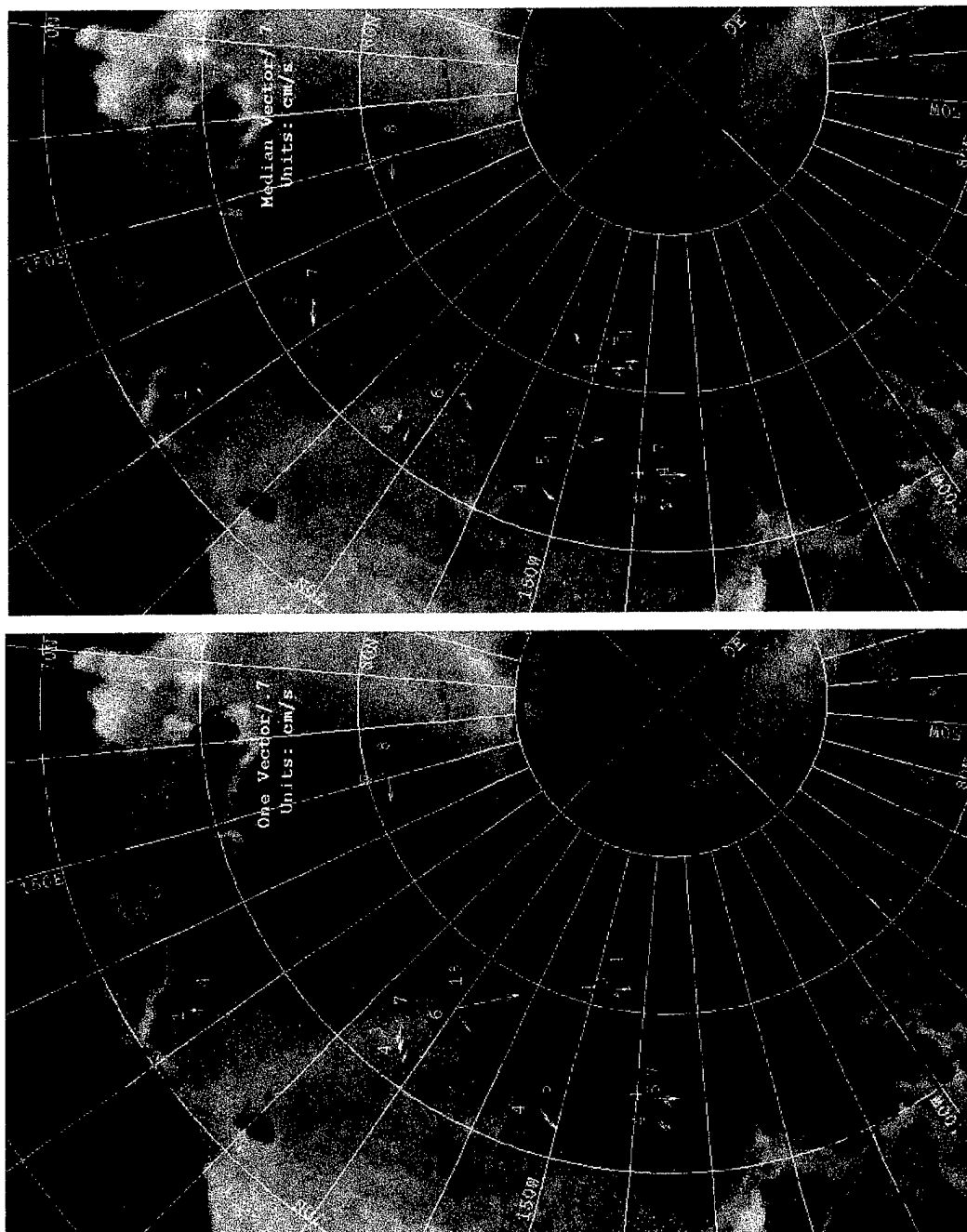


**Figure 9.** Closest and median SSM/I motion vector match using a 0.7 correlation for December 27<sup>th</sup>, 1999 at 1200Z.

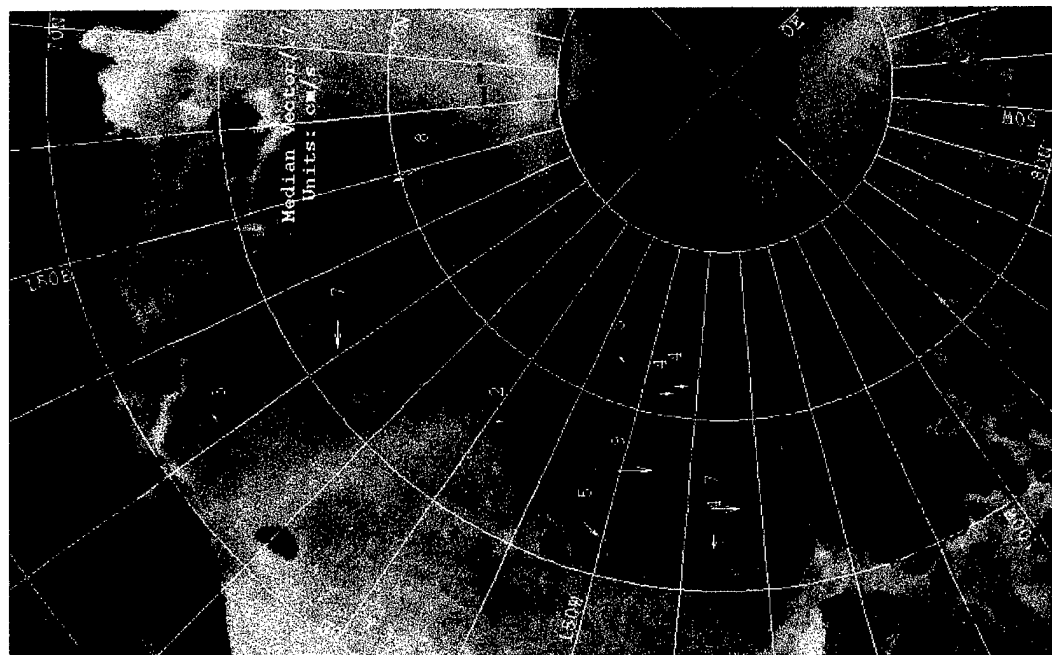
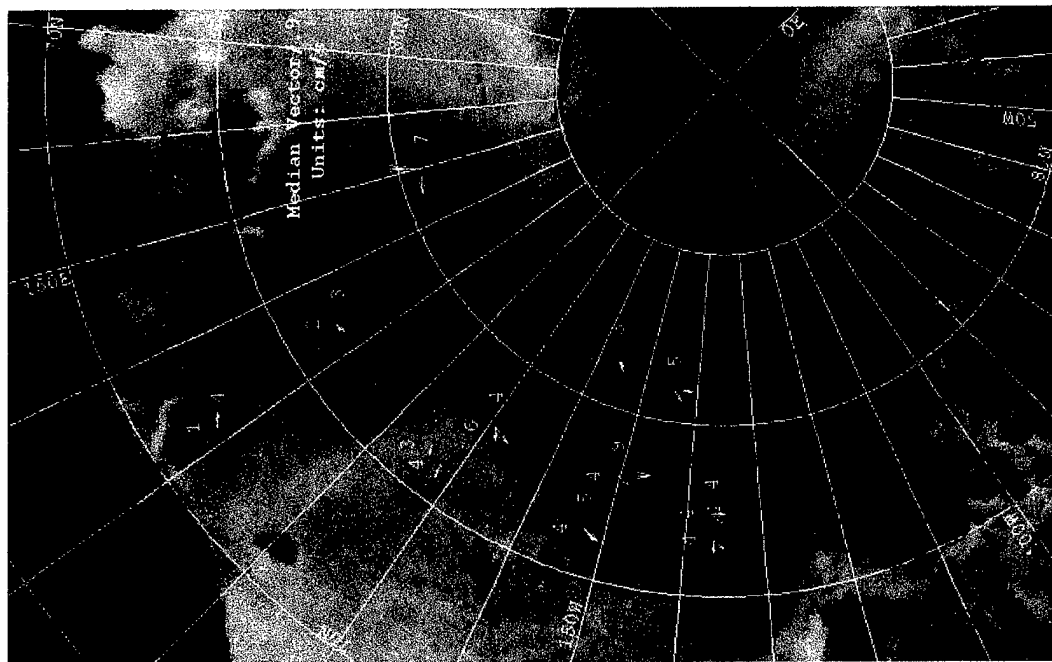


**Figure 10.** Median SSM/I motion vector match using a 0.7 and 0.9 correlation for December 27<sup>th</sup>, 1999 at 1200Z.

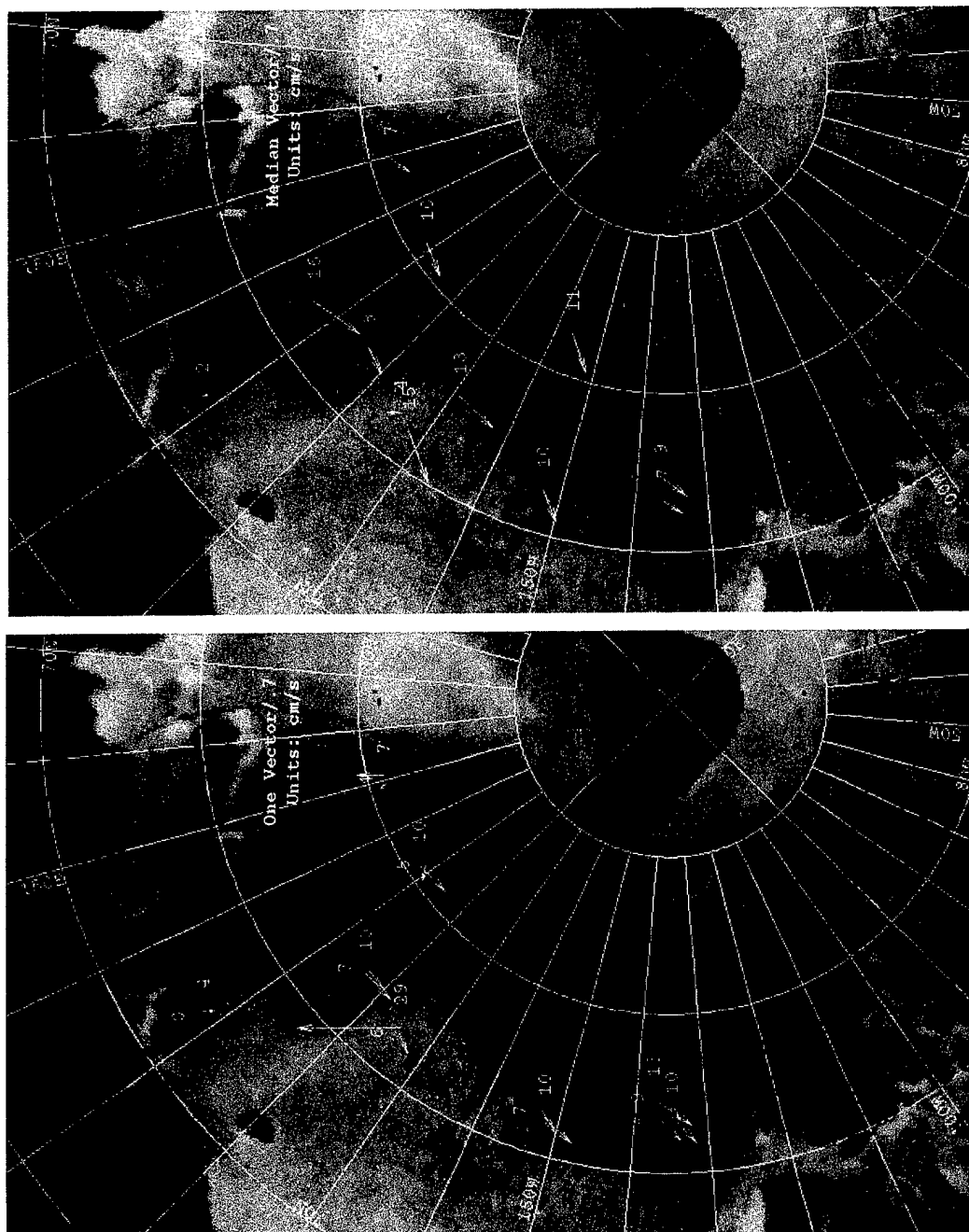


**Figure 11.** Closest and Median SSM/I motion vector match using a 0.7 correlation for December 28<sup>th</sup>, 1999 at 1200Z.

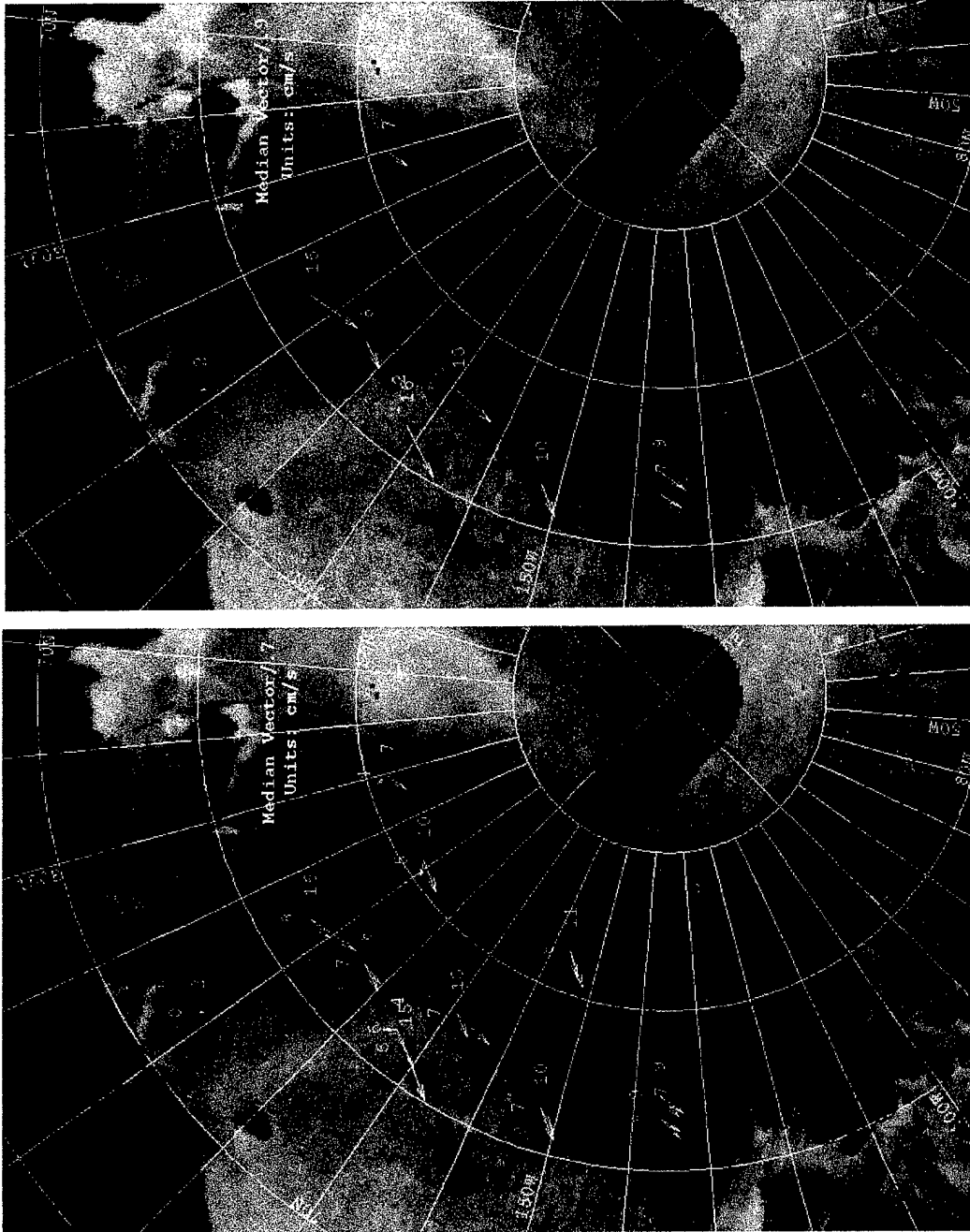
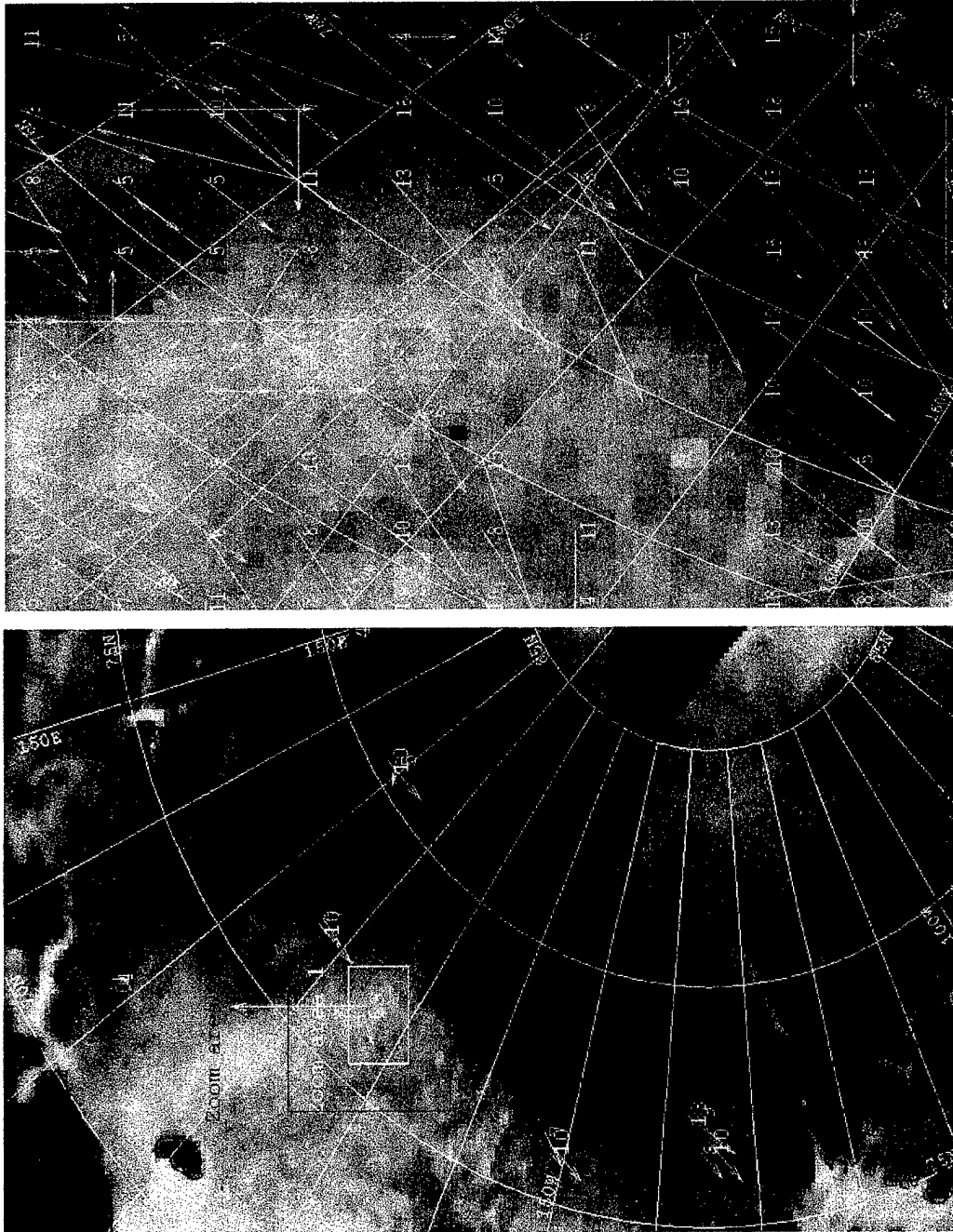
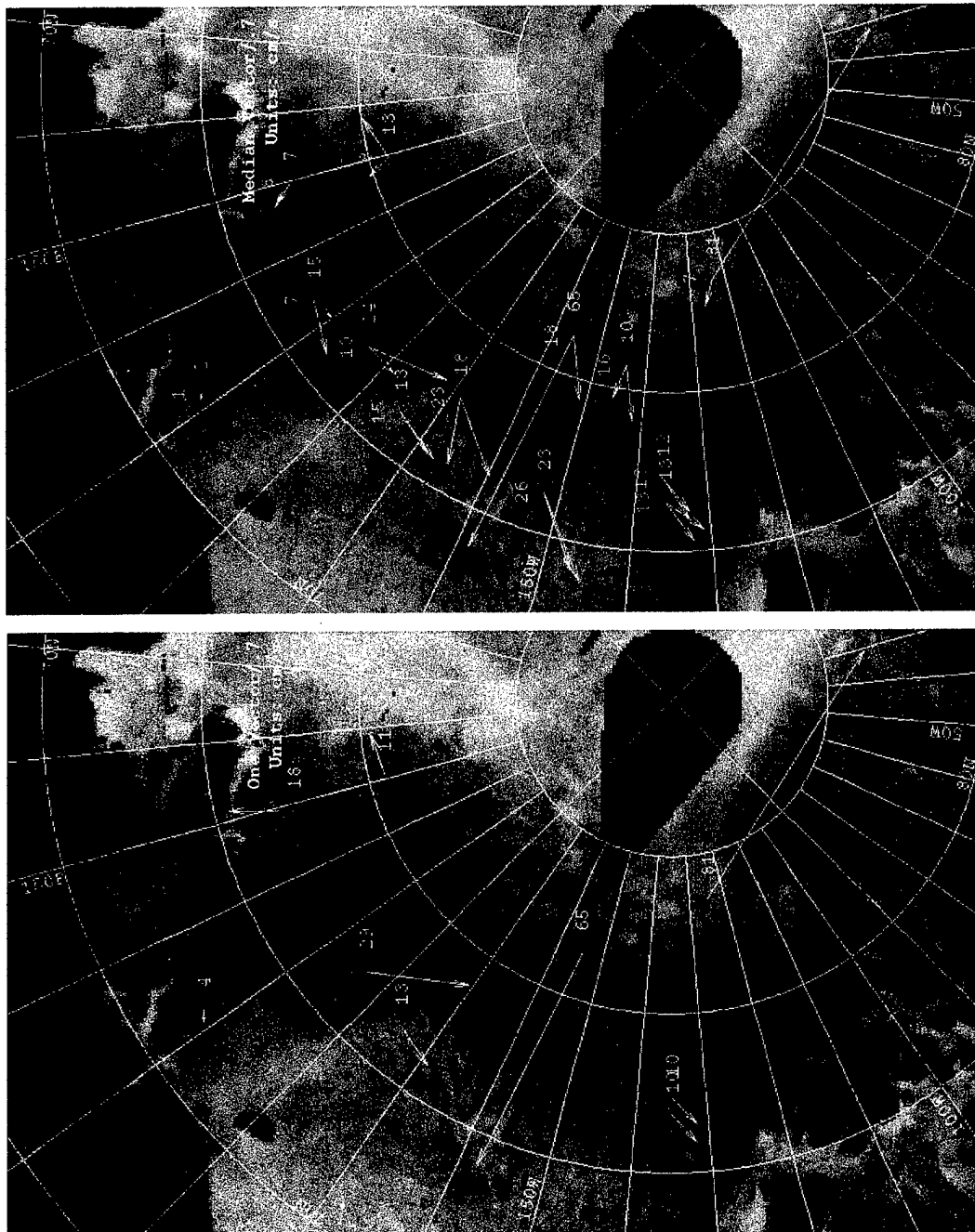


Figure 12. Median SSM/I motion vector match using a 0.7 and 0.9 correlation for December 28<sup>th</sup>, 1999 at 1200Z.





**Figure 13.** Highlighted area of closest SSM/I and buoy motion vector plot using a 0.7 correlation (L.H.S.). Area 1 zoomed (R.H.S.) for December 28th, 1999 at 1200Z.



**Figure 14.** Closest and median SSM/I motion vector match using a 0.7 correlation for December 29<sup>th</sup>, 1999 at 1200Z.

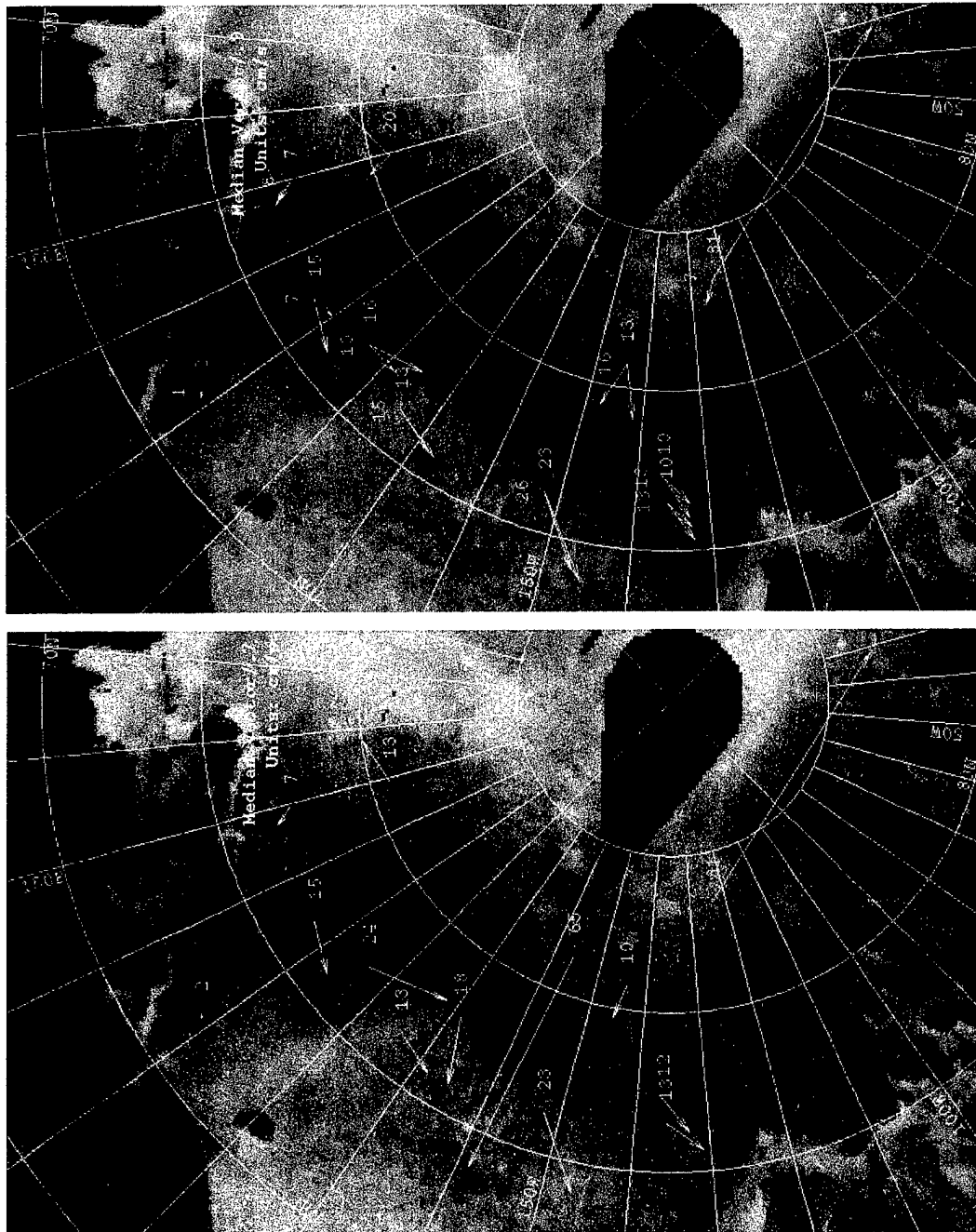


**Figure 15.** Median SSM/I motion vector match using a 0.7 and 0.9 correlation for December 29<sup>th</sup>, 1999 at 1200Z.

## **2. Case Study 2: January 15 - 16th, 2000 (SSM/I from NRL)**

Figure 16 is a full coverage plot of SSM/I and buoy motion vectors for the period of January 15th, 2000 at 1200Z and January 16<sup>th</sup>, 2000 at 0000Z. A low-pressure system is clearly detected by SSM/I and buoy motion vectors west of the Queen Elizabeth Islands. Very high SSM/I and buoy motion vectors cover an extensive region of the Western Arctic as the ice responds to very strong surface winds forced by a strong pressure gradient.

Figure 17 is a SSM/I and buoy motion vector match comparison plot using a 0.7 correlation threshold for January 15<sup>th</sup>, 2000 at 1200Z. Very few closest SSM/I and buoy motion vector pairs result in this case. The median SSM/I motion vector set provides several more matched pairs. Cyclonic motion vectors reflect the surface low pressure by the Queen Elizabeth Islands. One erroneous SSM/I vector from matching only the closest vector is retained using the median matching of SSM/I and buoy motion vectors.

Figure 18 is a SSM/I and buoy motion vector match comparison plot using a 0.7 and 0.9 correlation threshold for January 15<sup>th</sup>, 2000 at 1200Z. The 0.9 correlation threshold retains most of the good SSM/I and buoy pairs, including the cyclonic vectors associated with the low-pressure area. However, several good pairs from the 0.7 threshold do not pass the 0.9 threshold.

Figure 19 is a SSM/I and buoy motion vector match comparison plot using a 0.7 correlation threshold for January 16<sup>th</sup>, 2000 at 0000Z. The closest SSM/I motion vector match does very well for this 0000Z run. No significant differences in synoptic conditions are evident compared to the 1200Z composite on January 15<sup>th</sup>. More pairs

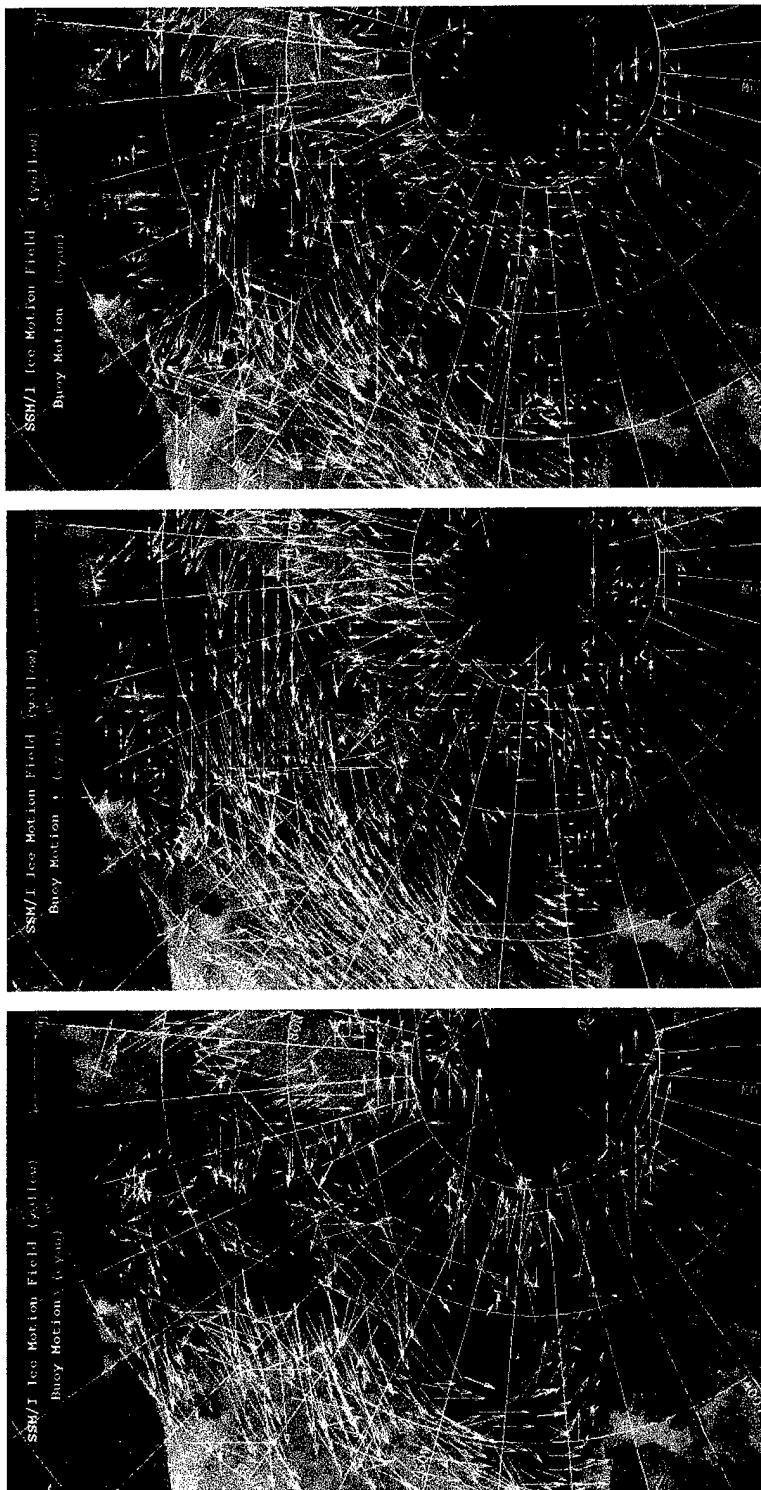
result from the median SSM/I and buoy motion vector matching, including two obvious erroneous pairs.

Figure 20 is a SSM/I and buoy motion vector match comparison plot using a 0.7 and 0.9 correlation threshold for January 16<sup>th</sup>, 2000 at 0000Z. The 0.9 correlation threshold removes all clearly erroneous SSM/I and buoy matched pairs and retains the good matches of the remaining pairs.

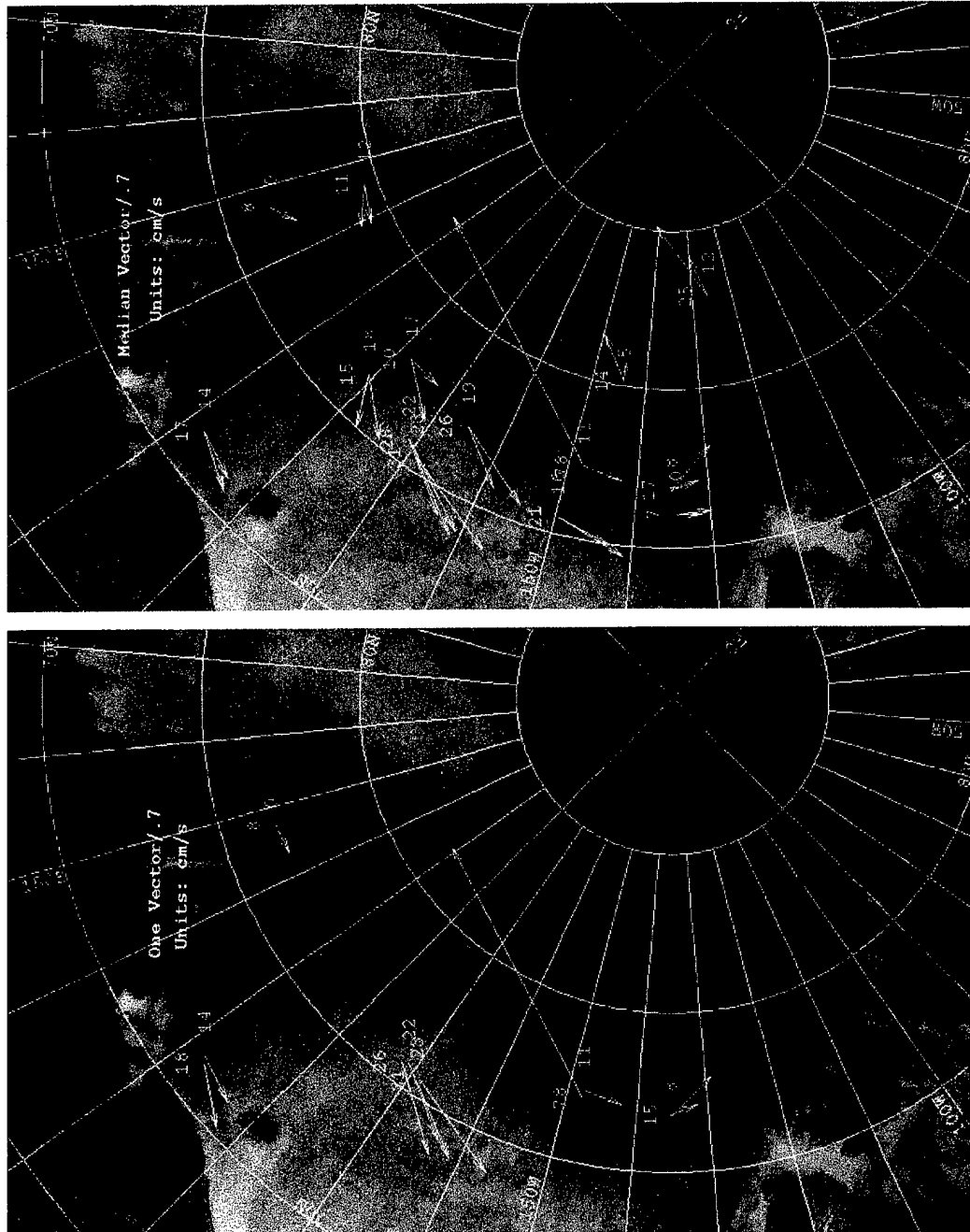
Figure 21 is a SSM/I and buoy motion vector match comparison plot using a 0.7 correlation threshold for January 16<sup>th</sup>, 2000 at 1200Z. The closest SSM/I motion vector match does very well. In this case, more pairs result from the median SSM/I vector, including some clearly erroneous pairs.

Figure 22 is a SSM/I and buoy motion vector match comparison plot using a 0.7 and 0.9 correlation threshold for January 16<sup>th</sup>, 2000 at 1200Z. The 0.9 correlation threshold removes all clearly erroneous SSM/I and buoy matched pairs and two reasonable matched pairs. Unlike the previous day, where motion values improved with the 0.9 correlation threshold, no improvement is apparent in motion values that pass the 0.9 correlation threshold.

***Summary for Case study 2 (NRL SSM/I data):*** The January 15 - 16<sup>th</sup> time frame displays high motions resulting from a constant strong pressure gradient. A closed low pressure remains stationary northwest of the Queen Elizabeth Islands. SSM/I motion vectors reflect both meteorological conditions very well. SSM/I and buoy motion pairs are numerous using all three methods. The composite for January 15<sup>th</sup> at 1200Z did not provide as many SSM/I and buoy motion vector pairs as January 16<sup>th</sup> at 0000Z and 1200Z. Further investigation revealed fewer buoys were available for January 15<sup>th</sup>.



**Figure 16.** Plotted SSM/I and buoy motion vectors for January 15<sup>th</sup>, at 1200Z and January 16<sup>th</sup>, 2000 at 0000Z and 1200Z.



**Figure 17.** Closest and median SSM/I motion vector match using a 0.7 correlation for January 15<sup>th</sup>, 2000 at 1200Z.

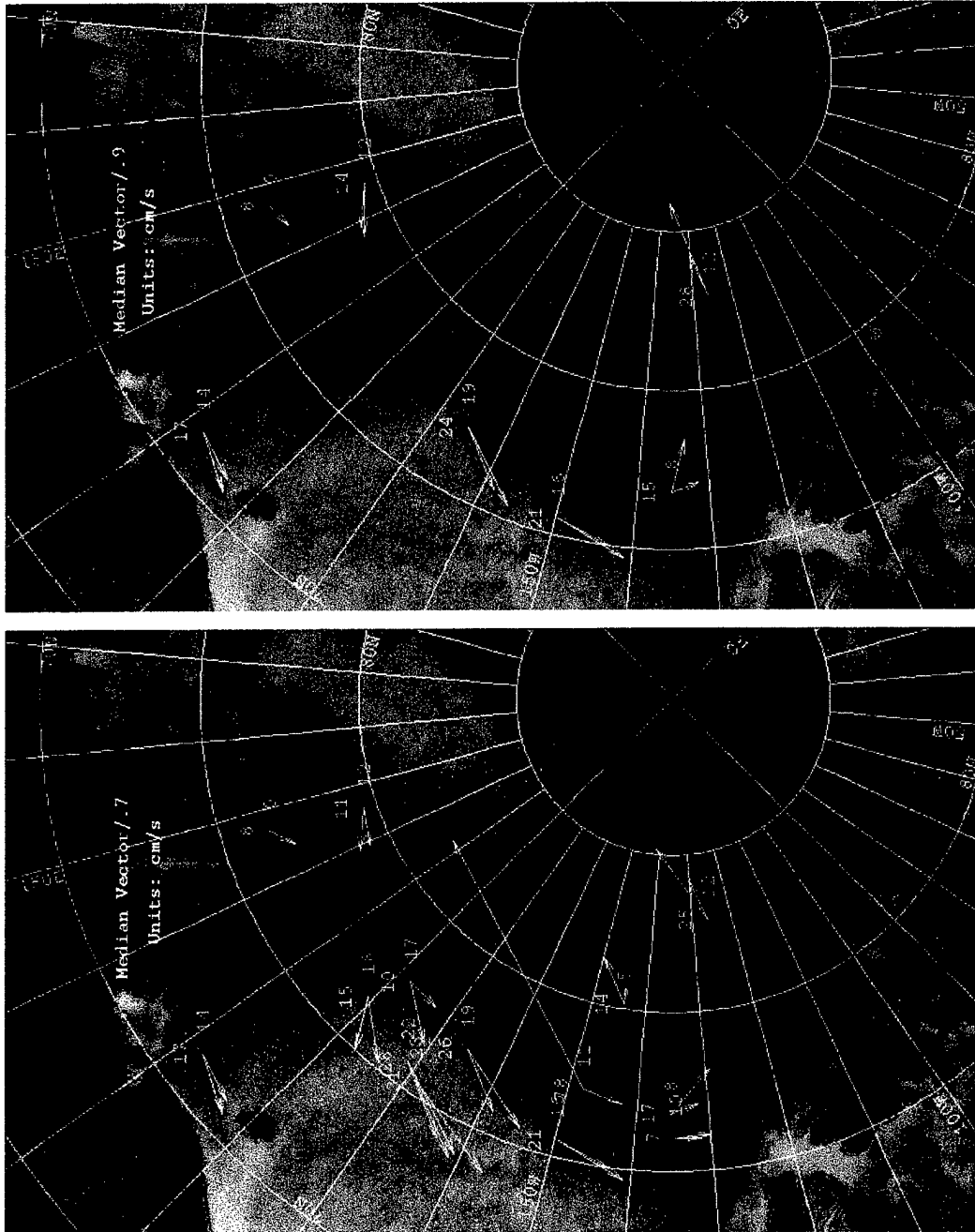


**Figure 18.** Median SSM/I motion vector match using a 0.7 and 0.9 correlation for January 15th, 2000 at 1200Z.



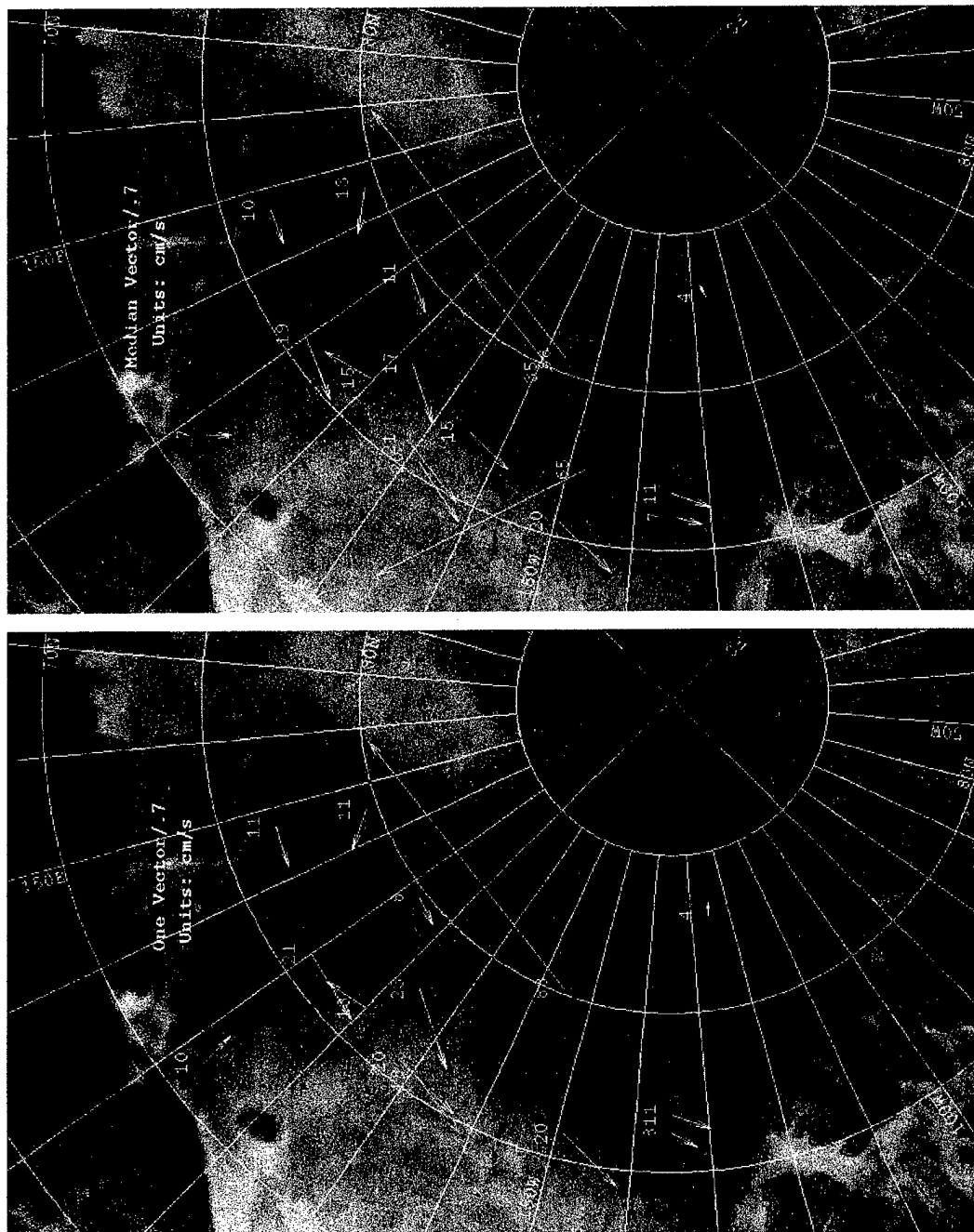


**Figure 19.** Closest and median SSM/I motion vector match using a 0.7 correlation for January 16<sup>th</sup>, 2000 at 0000Z.

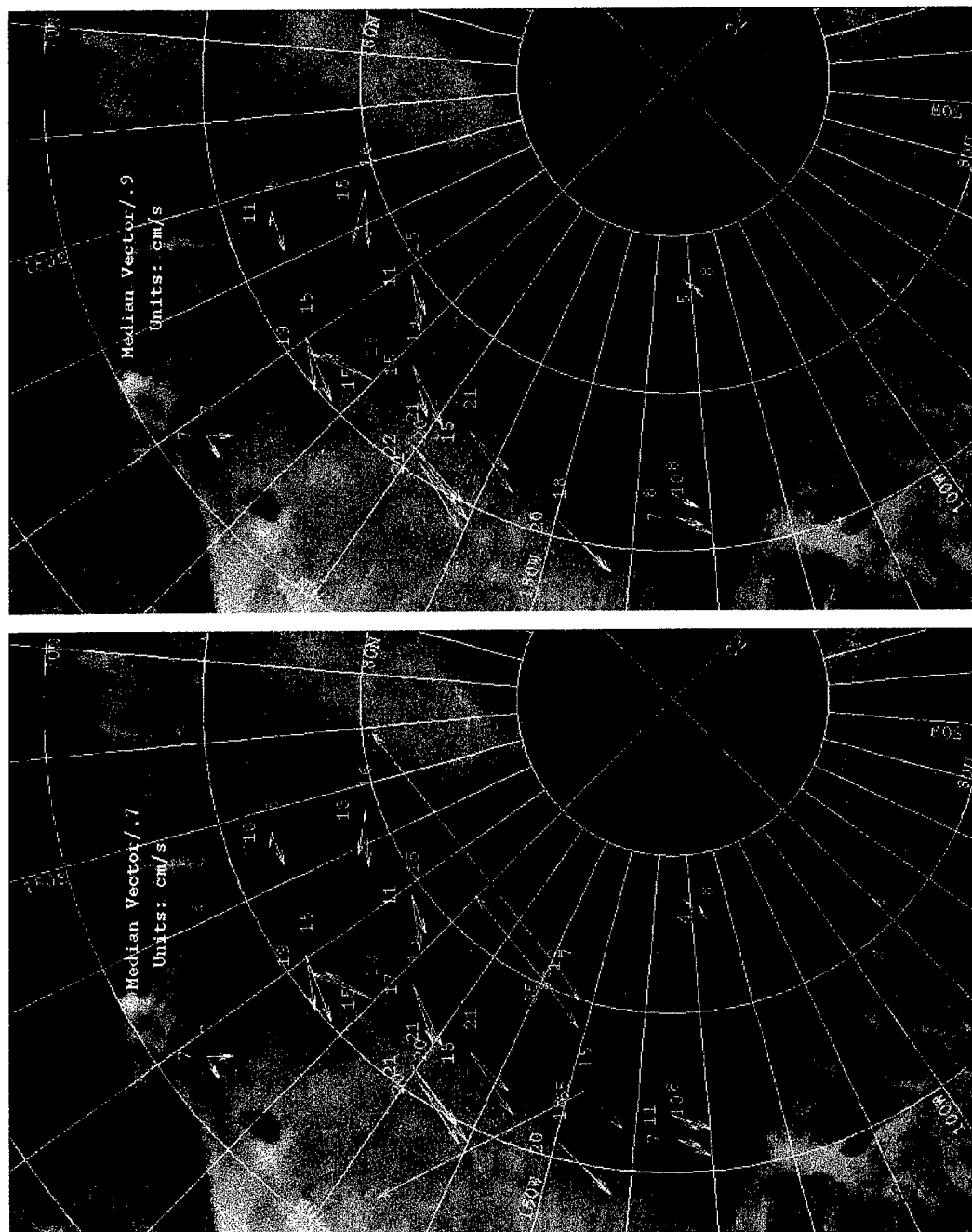


**Figure 20.** Median SSM/I motion vector match using a 0.7 and 0.9 correlation for January 16th, 2000 at 0000Z.

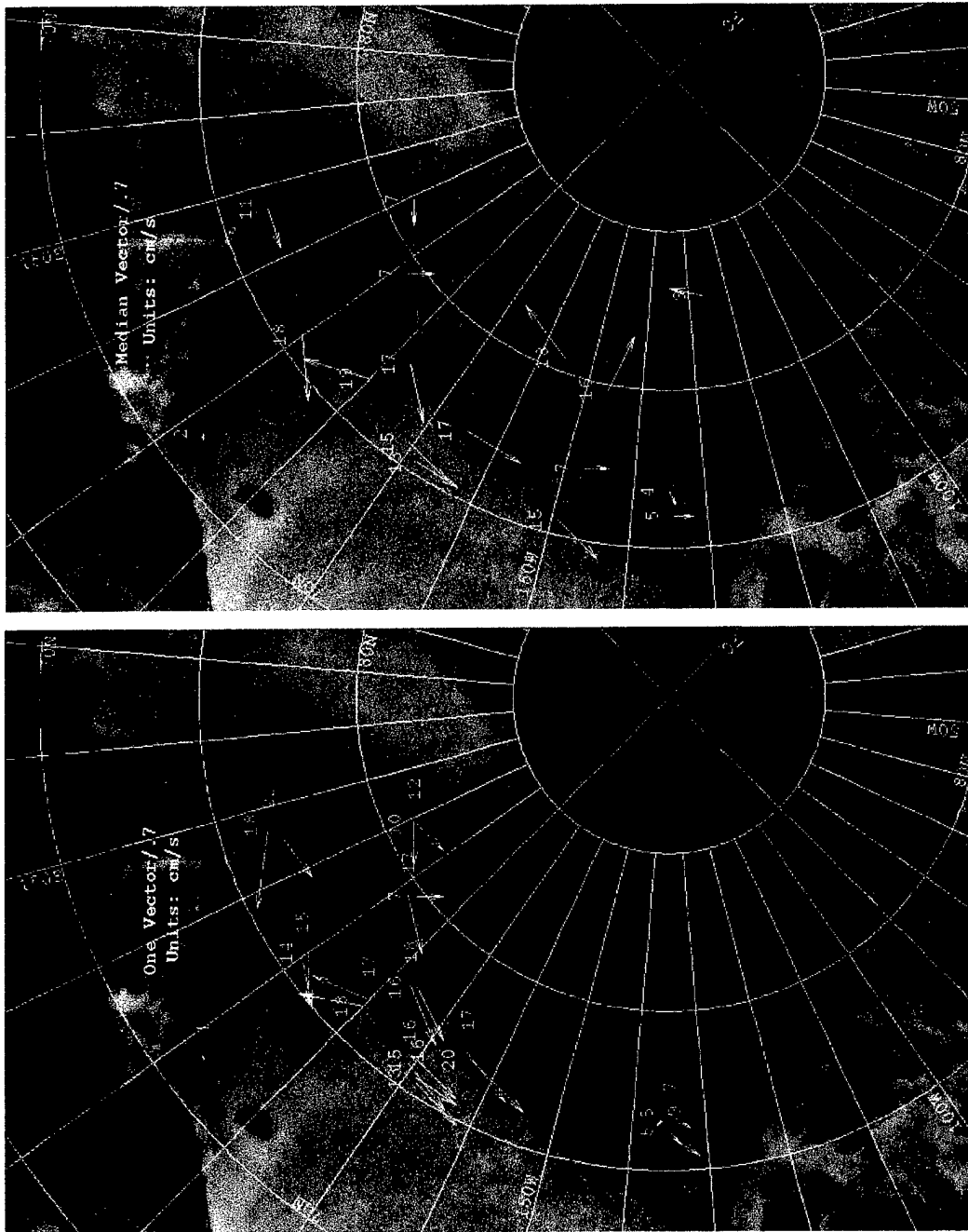


**Figure 21.** Closest and median SSM/I motion vector match using a 0.7 correlation for January 16<sup>th</sup>, 2000 at 1200Z.

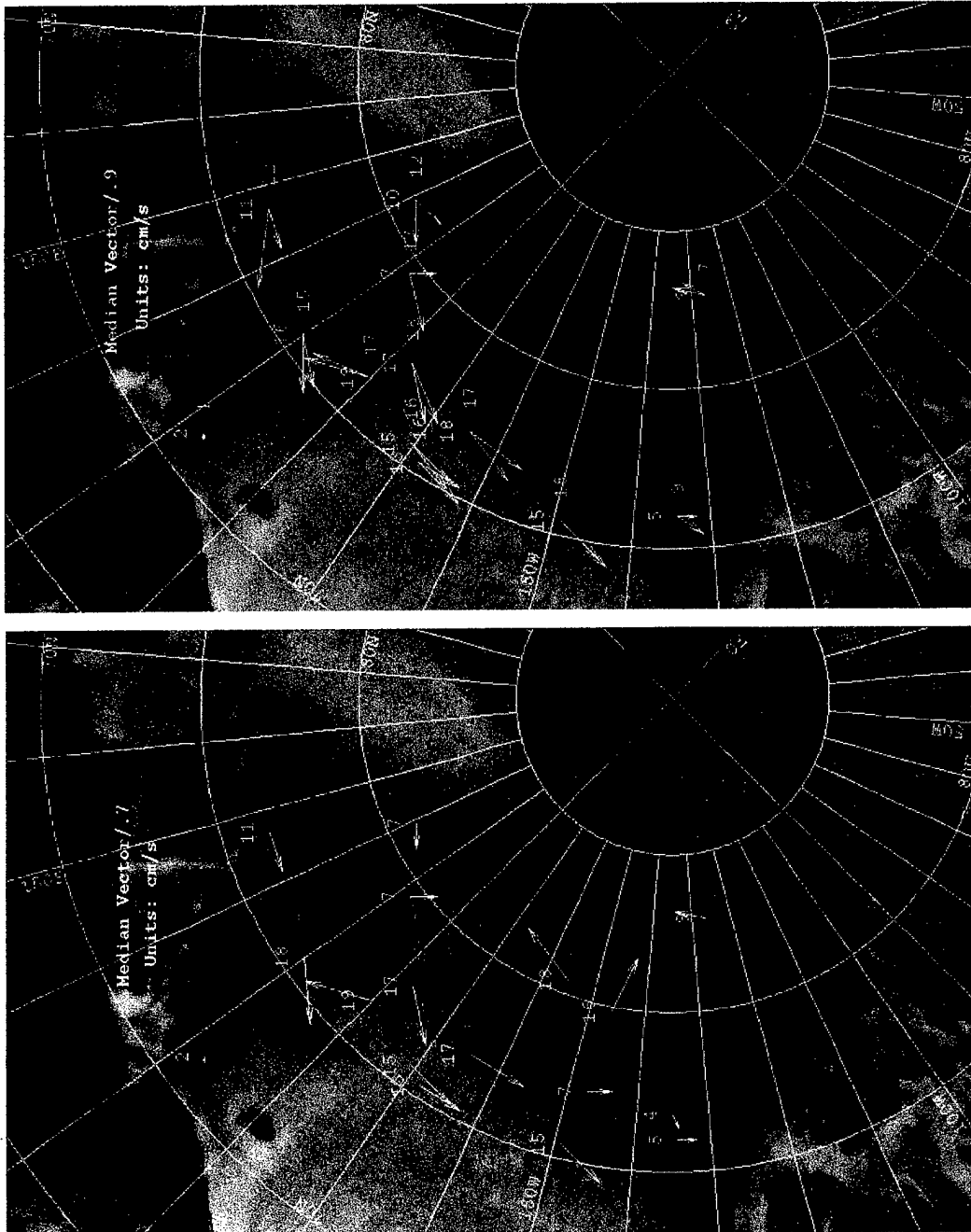


**Figure 22.** Median SSM/I motion vector match using a 0.7 and 0.9 correlation for January 16th, 2000 at 1200Z.

### **3. Case Study 3: February 17 - 18th, 2000 (SSM/I Data from NRL and FNMOC)**

Case 3 begins a transition from using solely NRL SSM/I data to FNMOC SSM/I data. The most important difference between the data sets is the compositing technique. NRL formatted data is composited using TeraScan while FNMOC formatted data is composited using the Meier ice-motion algorithm. TeraScan uses a more sophisticated bi-linear interpolation technique, while FNMOC uses a "drop-in-the-bucket" averaging technique. The same SSM/I orbital passes were selected and processed for both composite routines in Case Study 3.

The synoptic condition for Case Study 3 is vastly different from Cases 1 and 2. Buoy motions reflect light winds as the western Arctic is under the influence of a high-pressure ridge. Case Study 3 shows algorithm characteristics during a light motion regime. A comparison between NRL and FNMOC derived motion vectors are also described.

Figure 23 is a full coverage plot of SSM/I and buoy motion vectors for the period of February 18<sup>th</sup>, 2000 at 0000Z. The NRL plot is on the left hand side with the FNMOC plot on the right hand side. Buoy motions are very small due to light winds. With buoy motions less than 3 cm/s, the accuracy of derived SSM/I motion vectors is not expected to be high.

Differences between the NRL and FNMOC SSM/I motion vector plots are apparent in Figure 23. Though buoy motion vectors are small and hard to see due to slow motions the NRL vectors show buoy directions well. The FNMOC SSM/I motion

vectors are erratic and do not provide a sense of ice movement or agree with actual buoy direction.

Figure 24 is a full coverage plot of SSM/I and buoy motion vectors for the period of February 18<sup>th</sup>, 2000 at 1200Z. The NRL plot is on the left hand side with the FNMOC plot on the right hand side. Buoy motions remain low throughout this period. The only significant difference noted from 12 hours earlier is fewer SSM/I motion vectors are plotted for NRL and FNMOC. NRL SSM/I motion vectors continue to reflect the slow buoy motion whereas FNMOC SSM/I motion vectors do not reflect the buoy motion.

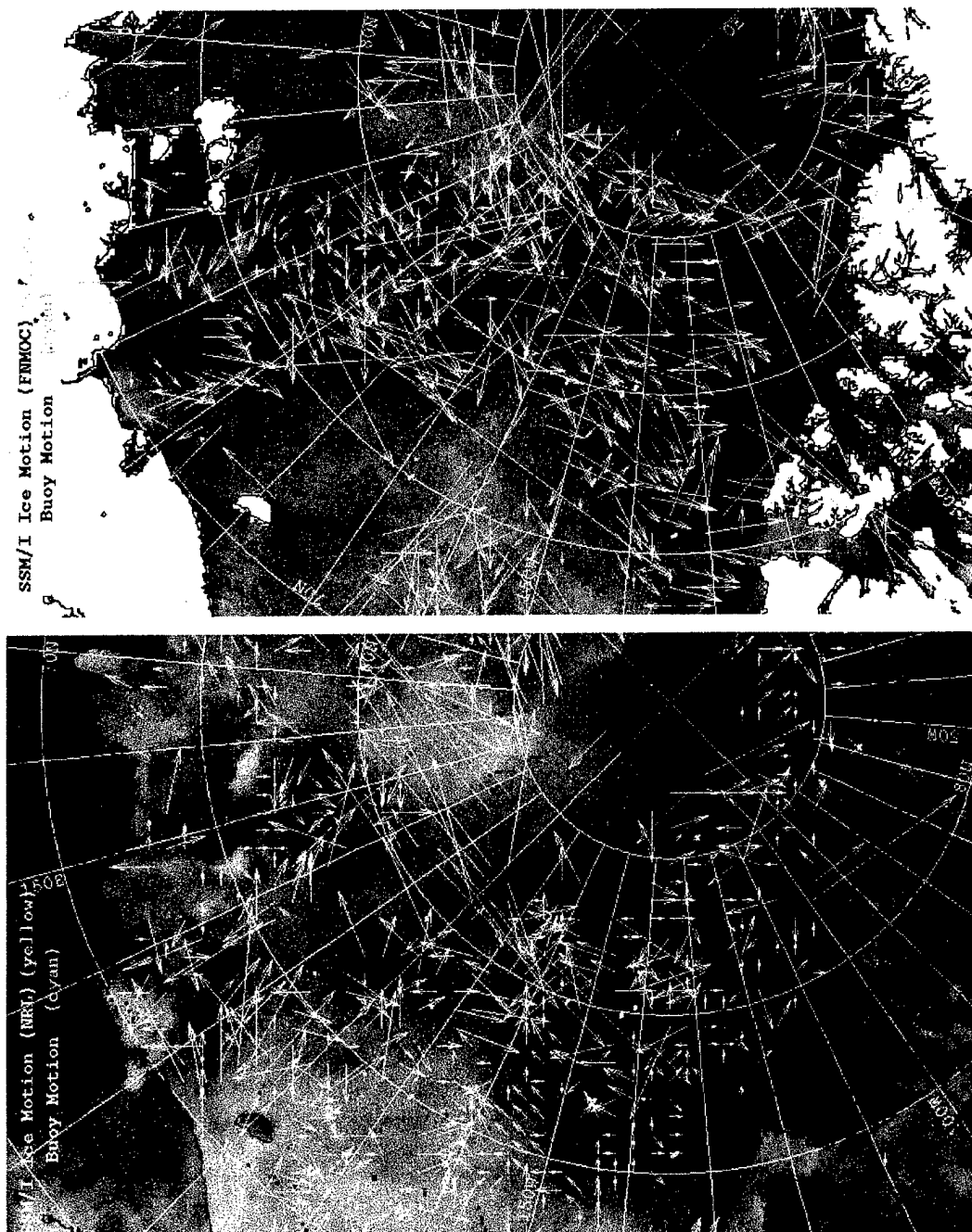
Figure 25 is a SSM/I and buoy motion vector match comparison plot using a 0.7 correlation threshold for February 18th, 2000 at 0000Z. The closest SSM/I motion vector pairs are plotted for NRL and FNMOC. No reliable pairs are evident. NRL SSM/I motion vectors do reflect buoy direction whereas FNMOC does not. An interesting point is that the SSM/I and buoy motion vector pairs for both plots are different. Since the same data was used in the compositing routines, the correlated pairs show that the different compositing routines produce significantly different motion vectors.

Figure 26 is a SSM/I and buoy motion vector match comparison plot using a 0.7 correlation threshold for February 18th, 2000 at 0000Z. The median SSM/I motion vector pairs are plotted for NRL and FNMOC. No discernible improvements are reflected in the NRL plot. The median matching of FNMOC SSM/I and buoy motion vectors results in several new pairs and the values match the buoys better than the closest buoy comparison.

Figure 27 is a SSM/I and buoy motion vector match comparison plot using a 0.9 correlation threshold for February 18th, 2000 at 0000Z. The SSM/I motion vector pairs

are plotted for NRL and FNMOC. No discernible improvements are reflected in either plot.

*Summary for Case study 3 (NRL and FNMOC SSM/I data):* The period of February 17 - 18<sup>th</sup> was selected to investigate the ice motion algorithm ability to detect ice motion during a light wind period. This period of time also provided an opportunity to directly compare NRL and FNMOC derived SSM/I motion vector results. As expected, SSM/I motion vector speeds are not accurate and directions are erratic due to the light ice motion conditions. There are clear SSM/I motion vector differences between NRL and FNMOC. Buoy motions are hard to see, but the NRL SSM/I vectors reflect buoy directional vectors. FNMOC SSM/I motion vectors are sparse and erratic, with no vector component matching with the buoys.



**Figure 23.** Plotted SSM/I and buoy motion vectors for February 18<sup>th</sup>, 2000 at 0000Z  
(NRL and FNMO SSM/I Data).



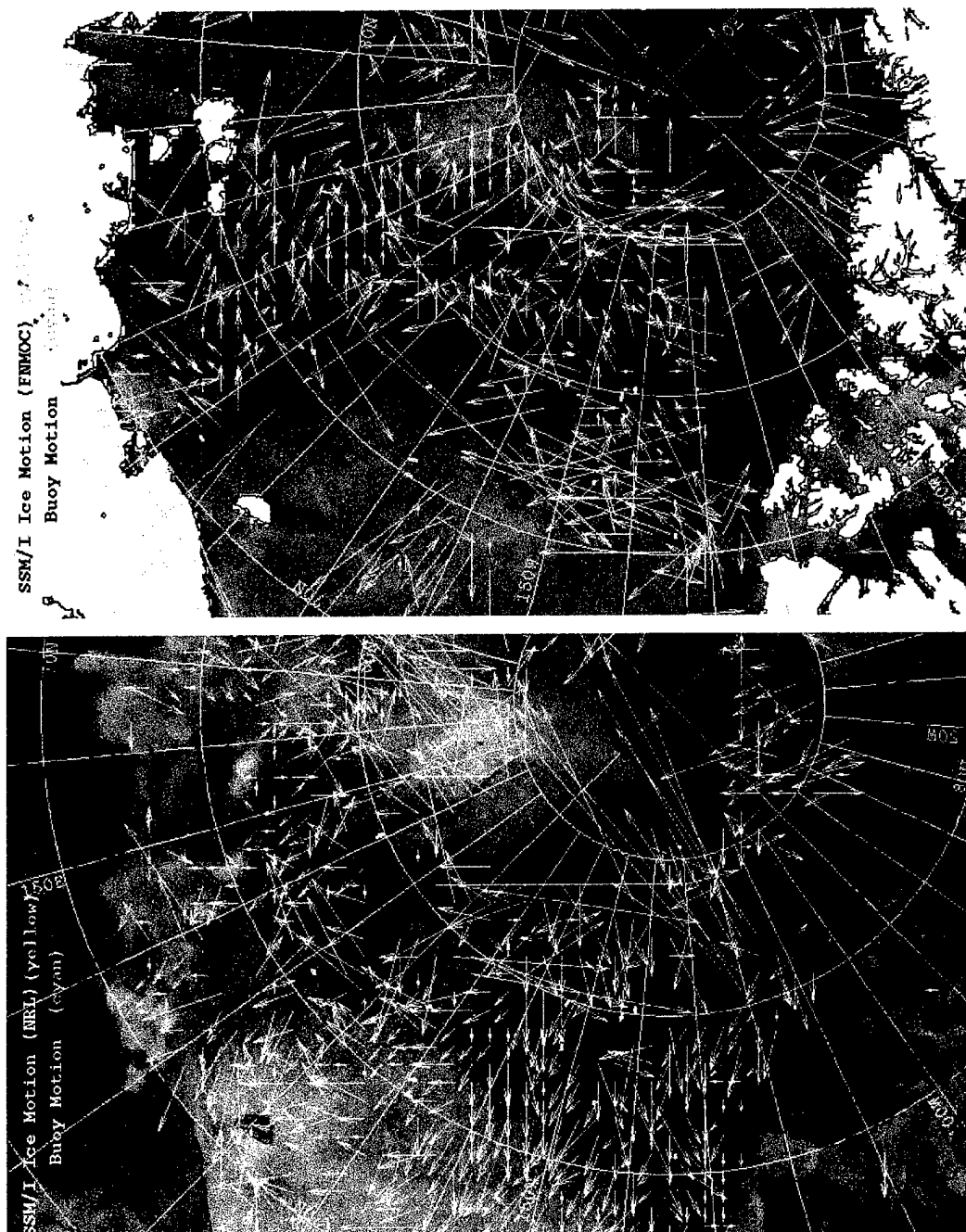


**Figure 24.** Plotted SSM/I and buoy motion vectors for February 18<sup>th</sup>, 2000 at 1200Z  
(NRL and FNMOC SSM/I Data).

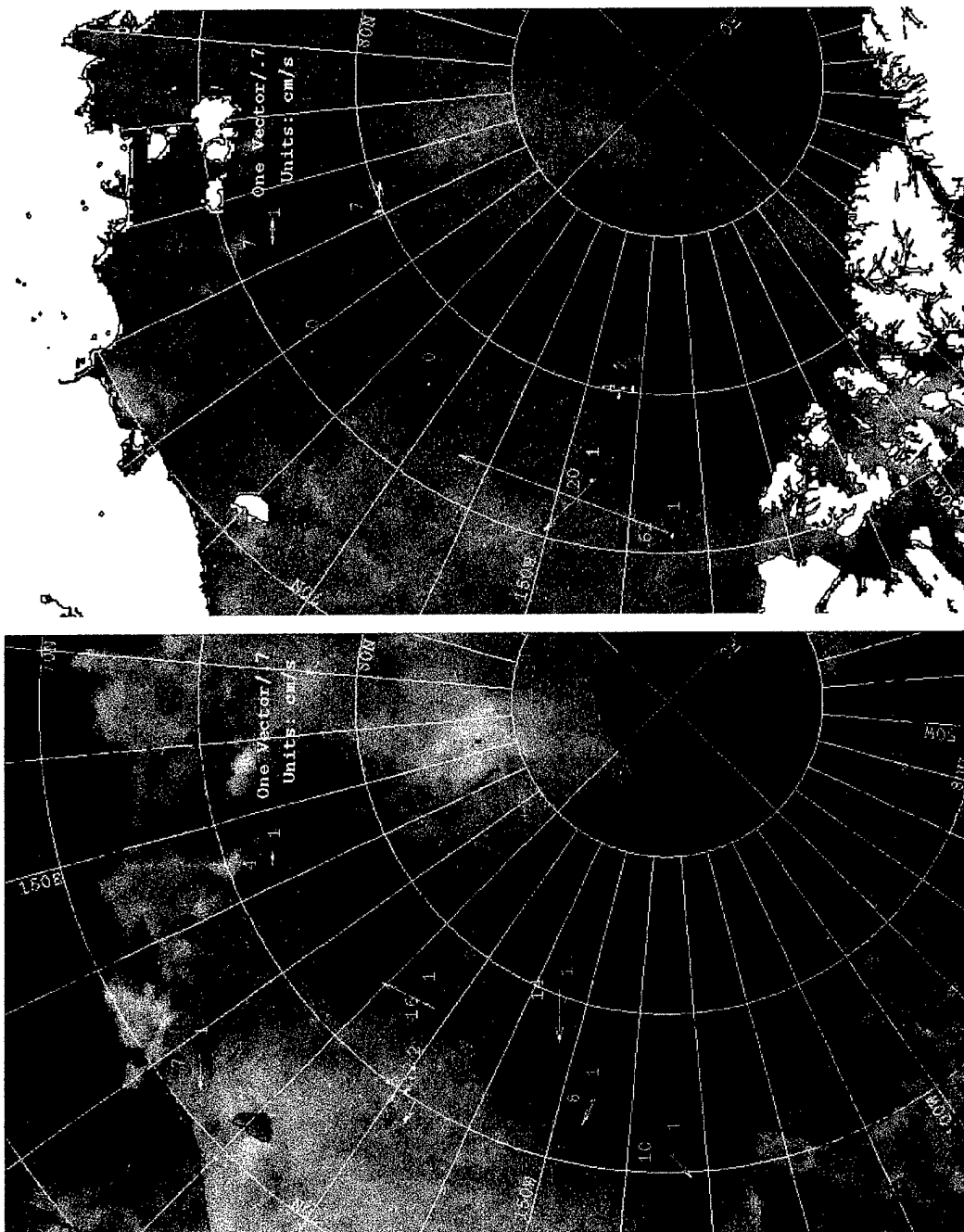


**Figure 25.** Closest SSM/I motion vector match using a 0.7 correlation for February 18<sup>th</sup>, 2000 at 0000Z (NRL and FNMOC SSM/I Data).

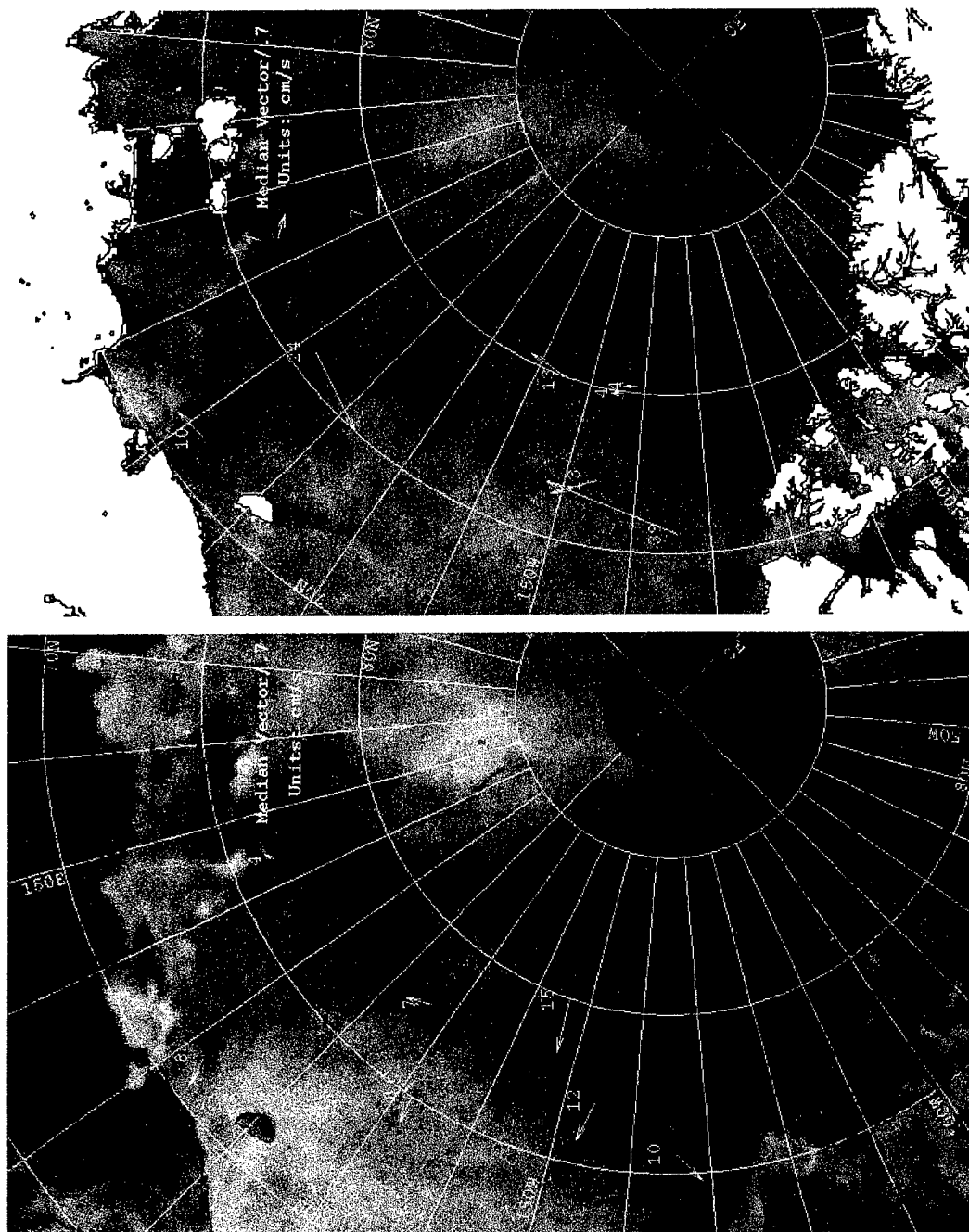


**Figure 26.** Median SSM/I motion vector match using a 0.7 correlation for February 18<sup>th</sup>, 2000 at 0000Z (NRL and FNMOC SSM/I Data).

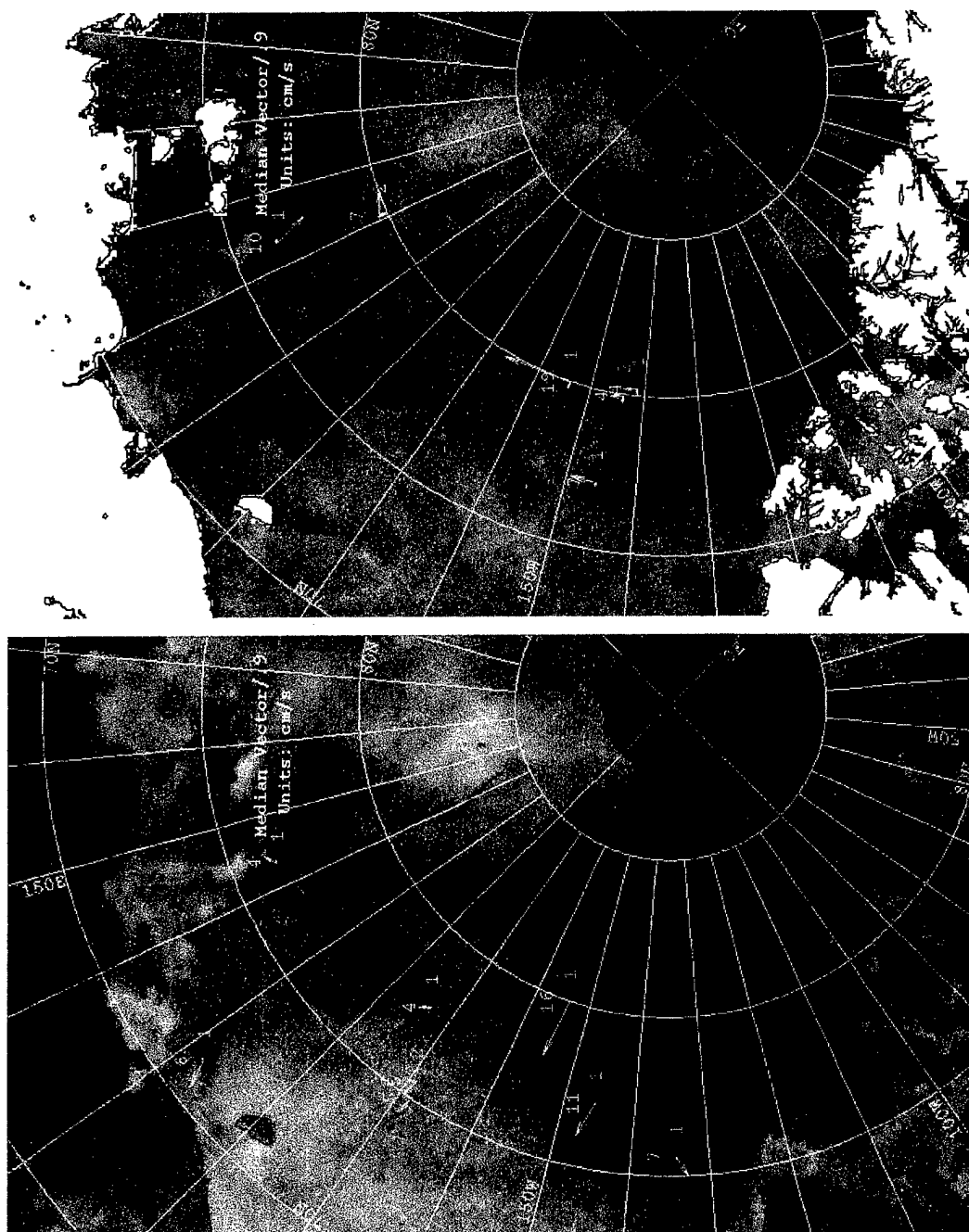


**Figure 27.** Median SSM/I motion vector match using a 0.9 correlation for February 18<sup>th</sup>, 2000 at 0000Z (NRL and FNMOC SSM/I Data).

#### **4. Case Study 4: March 06 - 08th, 2000 (SSM/I from FNMOC)**

Case Study 4 takes a direct look at composited FNMOC data using the ice motion algorithm. FNMOC SSM/I motion vectors in Case Study 3 resulted in no accurate SSM/I motion vectors. Case Study 4 is influenced by an intensifying high-pressure system over the Western Arctic and increasing surface winds that force high buoy motion speeds.

Figure 28 is a full coverage plot of SSM/I and buoy motion vectors for the period of March 06 - 08th, 2000 at 1200Z. SSM/I motion vectors provide a good indication of ice movement in the area of high buoy motions. There are several gaps in coverage as in Case Study 3.

Figure 29 is a SSM/I and buoy motion vector match comparison plot using a 0.7 correlation threshold for March 07th, 2000 at 1200Z. In contrast to Case Study 3, the closest SSM/I to buoy motion vector match does relatively well in areas of faster ice motion. SSM/I motion vector speeds and directions show a definite improvement due to high buoy motion speeds. The median vector match clearly adds value resulting in more pairs and SSM/I speed and direction values are in agreement with buoy values.

Figure 30 is a SSM/I and buoy motion vector match comparison plot using a 0.7 and 0.9 correlation threshold for March 07th, 2000 at 1200Z. Most of the SSM/I and buoy motion vector pairs are removed using the 0.9 correlation threshold. Only one of several apparently accurate matched pairs remain. This is very different from the NRL 0.9 correlation threshold results. NRL 0.9 correlated SSM/I and buoy motion vector pairs showed slightly better values compared to NRL 0.7 correlated plots. The 0.9 correlation threshold removes many good pairs from the FNMOC SSM/I and buoy motion vector pairs.

*Summary for Case study 4 (NRL and FNMOC SSM/I data):* The period of March 06 - 08<sup>th</sup> had an Arctic high-pressure that intensified to 1060 millibars. A section of the western Arctic had small buoy motions, whereas north and west of Wrangel Island displayed very high buoy motions. There are large gaps in SSM/I motion vector coverage as was also seen in Case Study 3.

The FNMOC median 0.7 correlation threshold plots provide much better coverage in SSM/I and buoy motion vector pairs than the median 0.9 correlation threshold. The 0.9 correlation threshold removed most SSM/I and buoy motion vector pairs. This is not true for the NRL composited data. In Case Studies 1 and 2, the 0.7 and 0.9 correlations provided good SSM/I and buoy motion vector pairs, with the 0.9 correlation threshold providing slightly better values. This suggests that under the FNMOC compositing, very few vectors have a correlation greater than about 0.7.

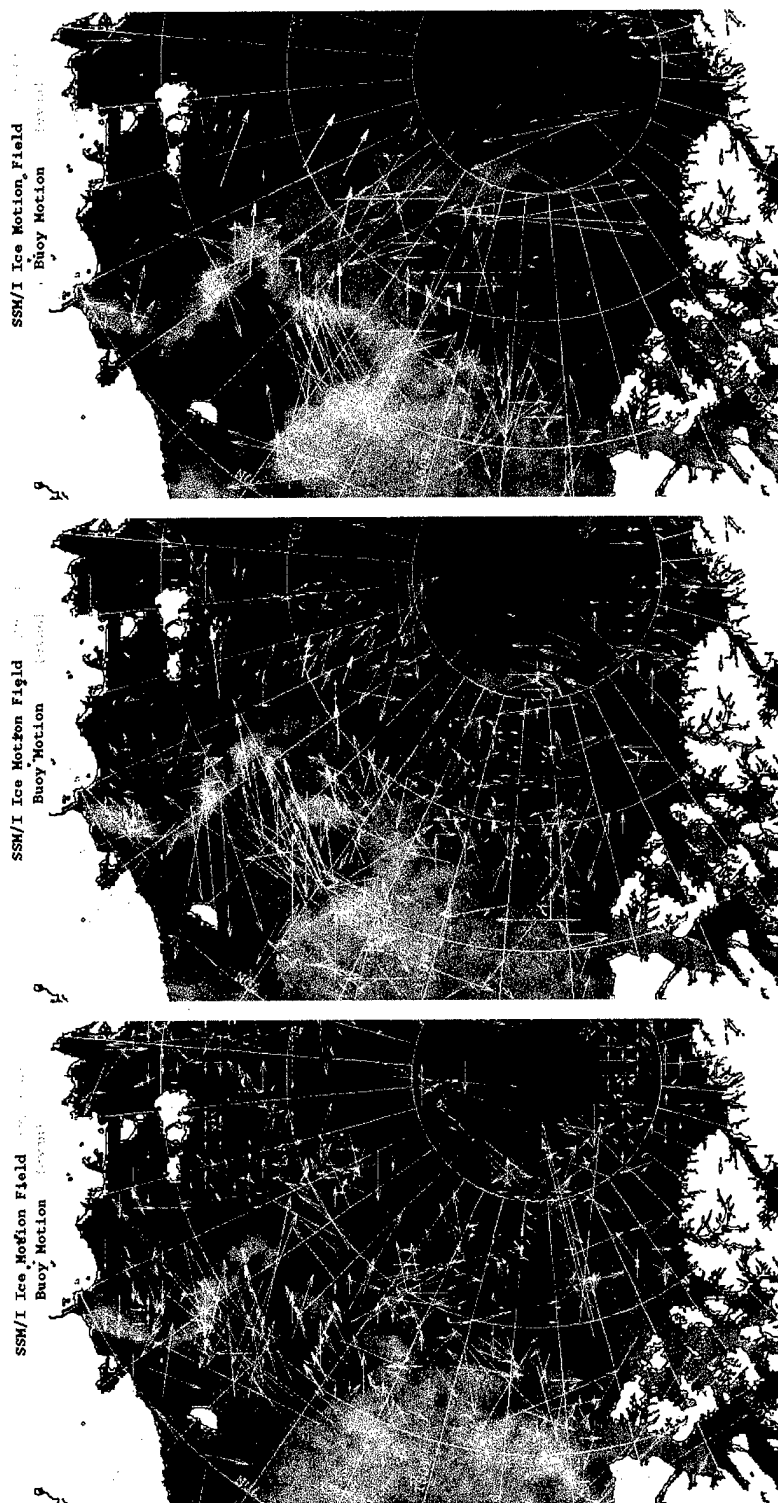
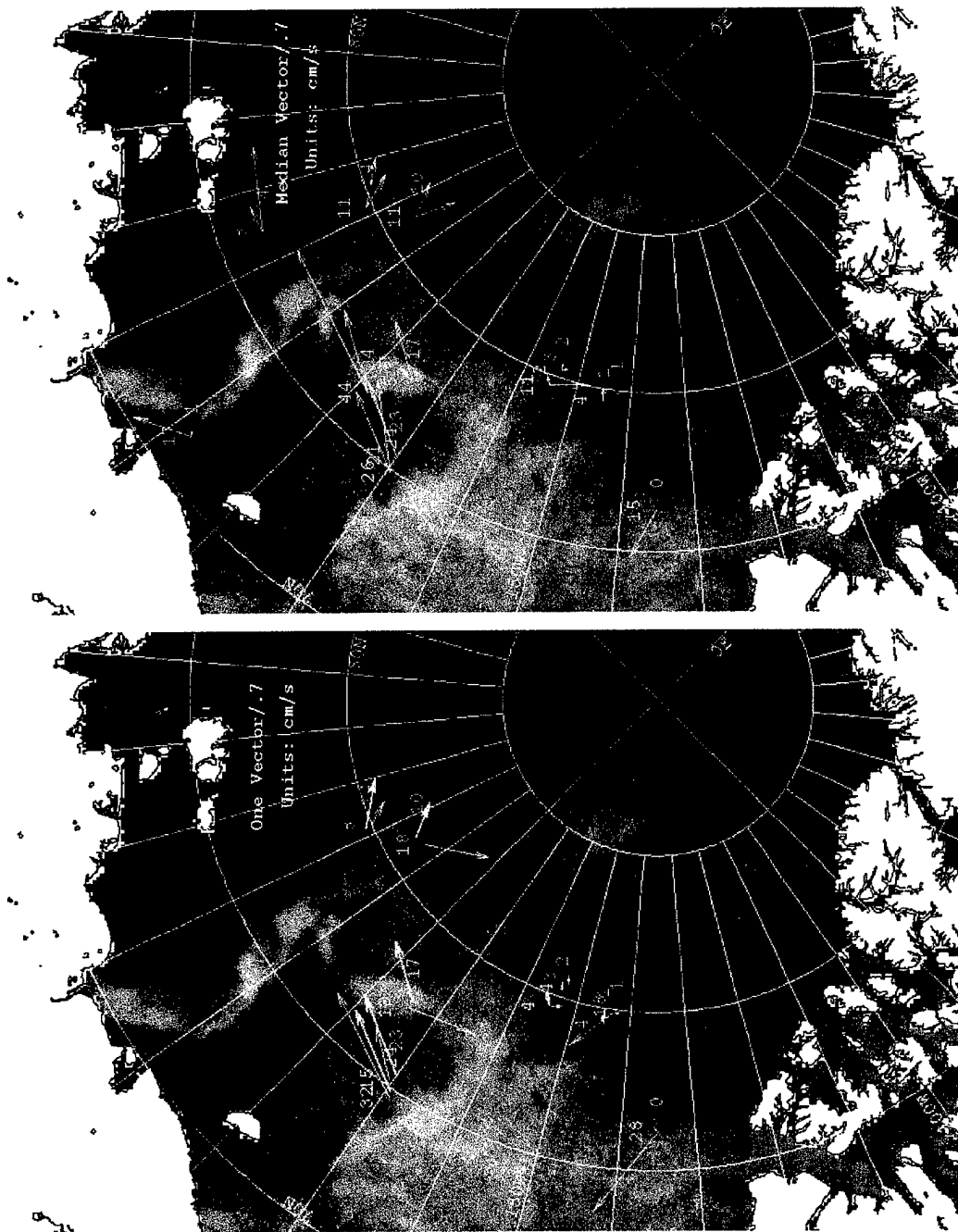
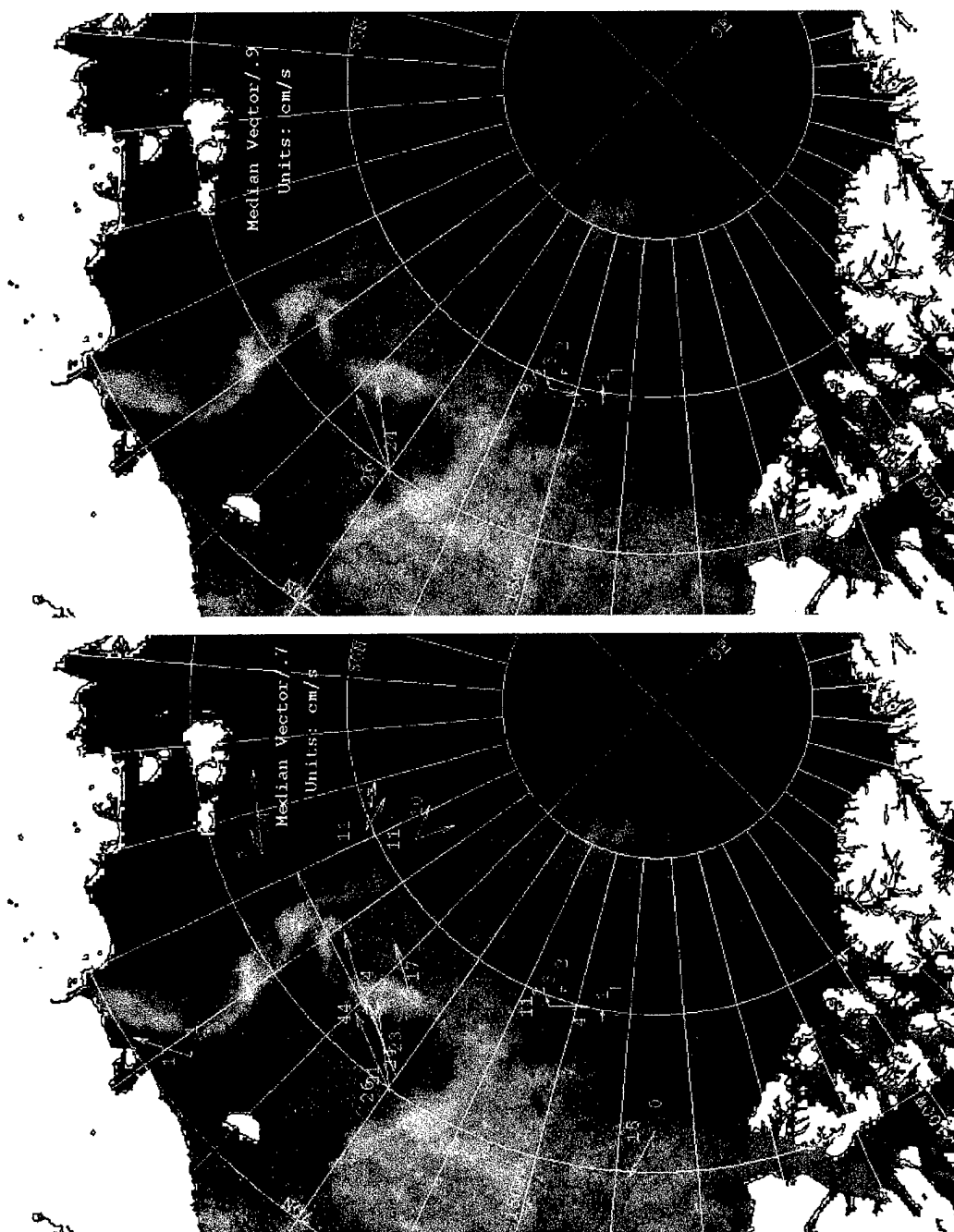


Figure 28. Plotted SSM/I and buoy motion vectors for March 06 - 08th, 2000 at 1200Z  
(FNMOC SSM/I Data).



**Figure 29.** Closest and median SSM/I motion vector match using a 0.7 correlation for March 07th, 2000 at 1200Z (FNMOC SSM/I Data).





**Figure 30.** Median SSM/I motion vector match using 0.7 and 0.9 correlation for March 07th, 2000 at 1200Z (FNMOC SSM/I Data).

## **B. SUMMARY STATISTICS**

Tables 5 through 8 provide normalized summary statistics derived from the 0.7 and 0.9 correlation thresholds as applied to the median SSM/I and buoy motion vector pairs for December through May. A Normalized Speed (NS) value is defined by dividing the SSM/I speed by the buoy speed. A NS value equal to 1.0 indicates perfect agreement with the buoy speed. The NS is multiplied by 100% for these tables. The Relative Direction (RD) is defined as the relative difference between the SSM/I and buoy derived directions.

Table 5 contains summary statistics for NRL composited data using the 0.7 correlation threshold. NS values between 80 - 120% are defined as good. As buoy speed increased, so do good NS percentages. For Table 5, there were 447 SSM/I and buoy pairs with ice motion speeds between 7.5 - 15.0 cm/s. 34.2% of those pairs fall within the 80 - 120 % NS range. Of the total pairs, 40.9 % have normalized speed values greater than 200%. Almost all of these bad NS values had buoy speeds between 0 - 7.5 cm/s. RD values of  $\pm 30^\circ$  are defined as good. As buoy speeds increased, so did the good RD percentages.

**Table 5. Normalized Speed and Relative Direction statistics for the 0.7 correlation threshold December 01, 1999 to February 29, 2000. (NRL data)**

	Total Pairs	Buoy Speed (cm/s)			
Normalized Speed	2066	0 - 7.5 1468	7.5 - 15.0 447	15.0 - 22.5 121	> 22.5 30
0 - 50%	203(9.8%)	134(9.1%)	50(11.2%)	15(12.4%)	4(13.3%)
50 - 80%	215(10.4%)	121(8.2%)	68(15.2%)	19(15.7%)	7(23.3%)
<b>80 - 120%</b>	<b>379(18.5%)</b>	<b>163(11.1%)</b>	<b>153(34.2%)</b>	<b>53(43.8%)</b>	<b>10(33.3%)</b>
120 - 150%	208(10.1%)	97(6.6%)	88(19.7%)	19(15.7%)	4(13.3%)
150 - 200%	217(10.5%)	158(10.8%)	48(10.7%)	8(6.6%)	3(10.0%)
<b>&gt; 200%</b>	<b>844(40.9%)</b>	<b>795(54.2%)</b>	<b>40(8.9%)</b>	<b>7(5.8%)</b>	<b>2(6.7%)</b>
Relative Direction +/-	2066	1468	442	125	31
0 - 30°	939(45.5%)	521(35.5%)	302(68.3%)	91(72.8%)	25(80.6%)
30 - 90°	681(33.0%)	548(37.3%)	108(24.4%)	20(16.0%)	5(16.1%)
90 - 180°	446(21.6%)	399(27.2%)	32(7.2%)	14(11.2%)	1(3.2%)

Table 6 contains summary statistics for NRL composited data using the 0.9 correlation threshold. As buoy speed increased, so do the good NS percentages. For Table 6, there were 338 SSM/I and buoy pairs with ice motion speeds between 7.5 - 15.0 cm/s. 36.4% of those pairs fall within the 80 - 120 % NS range. Of the total pairs, 39.6 % have normalized speed values greater than 200%. As in table 5, most bad NS values had buoy speeds between 0 - 7.5 cm/s. As buoy speeds increased, so did the good RD percentage values.

**Table 6. Normalized Speed and Relative Direction statistics for the 0.9 correlation threshold December 01, 1999 to February 29, 2000. (NRL data)**

	Total Pairs	Buoy Speed (cm/s)			
Normalized Speed	1618	0 - 7.5 1192	7.5 - 15.0 338	15.0 - 22.5 79	> 22.5 19
0 - 50%	196(12.1%)	142(11.9%)	38(11.2%)	13(16.5%)	3(15.8%)
50 - 80%	155(9.6%)	76(6.4%)	63(18.6%)	12(15.2%)	4(21.1%)
<b>80 - 120%</b>	<b>317(19.6%)</b>	<b>146(12.2%)</b>	<b>123(36.4%)</b>	<b>40(50.6%)</b>	<b>8(42.1%)</b>
120 - 150%	144(8.9%)	66(5.5%)	65(19.2%)	11(13.9%)	2(10.5%)
150 - 200%	165(10.2%)	145(12.2%)	29(8.6%)	1(1.3%)	0(0%)
<b>&gt; 200%</b>	<b>641(39.6%)</b>	<b>617(51.8%)</b>	<b>20(5.9%)</b>	<b>2(2.5%)</b>	<b>2(10.5%)</b>
Relative Direction +/-	1618	1182	327	90	19
0 - 30°	681(42.1%)	405(34.3%)	207(63.3%)	56(62.2%)	13(68.4%)
30 - 90°	541(33.4%)	433(36.6%)	88(26.9%)	14(15.6%)	6(31.6%)
90 - 180°	396(24.5%)	344(29.1%)	32(9.8%)	20(22.2%)	0(0%)

As shown in the case study analysis, applying the 0.9 correlation threshold to NRL composited data resulted in slightly better SSM/I and buoy motion vector values. This is also evident in Tables 5 and 6. Care must be taken when viewing statistics of buoy speeds greater than 22.5 cm/s due to the limited number of occurrences.

Table 7 contains summary statistics for FNMOC composited data using the 0.7 correlation threshold. NS values between 80 - 120% are defined as good. NS percentage values only increased for the 7.5 - 15.0 cm/s range of buoy speed. There were 221 SSM/I and buoy pairs with ice motion speeds between 7.5 - 15.0 cm/s and 26.2% of these pairs fall within the 80 - 120 % NS range. Of the total pairs, 45.1 % have normalized speed values greater than 200%. RD values of  $\pm 30^\circ$  are defined as good. As buoy speeds increased, the RD percentages did not always increase for the FNMOC data.

**Table 7. Normalized Speed and Relative Direction statistics for the 0.7 correlation threshold December 01, 1999 to February 29, 2000. (FNMOC data).**

	Total Pairs	Buoy Speed (cm/s)			
Normalized Speed	1033	0 - 7.5 731	7.5 - 15.0 221	15.0 - 22.5 64	> 22.5 17
0 - 50%	154(14.9%)	66(9.05)	60(27.1%)	23(35.9%)	5(29.4%)
50 - 80%	95(9.2%)	52(7.1%)	31(14.0%)	8(12.5%)	4(23.5%)
<b>80 - 120%</b>	<b>146(14.1%)</b>	<b>70(9.6%)</b>	<b>58(26.2%)</b>	<b>15(23.4%)</b>	<b>3(17.6%)</b>
120 - 150%	73(7.1%)	45(6.2%)	23(10.4%)	3(4.7%)	2(11.8%)
150 - 200%	99(9.6%)	69(9.4%)	21(9.5%)	7(10.9%)	2(11.8%)
<b>&gt; 200%</b>	<b>466(45.1%)</b>	<b>429(58.7%)</b>	<b>28(12.7%)</b>	<b>8(12.5%)</b>	<b>1(5.9%)</b>
Normalized Direction +/-	1033	731	221	64	17
0 - 30°	288(27.9%)	170(23.3%)	83(37.6%)	26(40.7%)	9(52.9%)
30 - 90°	345(33.4%)	258(35.3%)	70(31.7%)	14(21.9%)	3(17.6%)
90 - 180°	400(38.8%)	303(41.4%)	68(30.8%)	24(37.5%)	5(29.4%)

Table 8 contains summary statistics for FNMOC composited data using the 0.9 correlation threshold. NS percentage values for the 7.5 - 15.0 cm/s range of buoy speed are worse than those reflected in Table 7. For Table 8, there were 164 SSM/I and buoy pairs with ice motion speeds between 7.5 - 15.0 cm/s. Of the total pairs, 39.7 % have normalized speed values greater than 200%. Almost all of these values had buoy speeds between 0 - 7.5 cm/s. This is 3.6 % worse than using the 0.7 correlation threshold. As in Table 7, most of these values had buoy speeds between 0 - 7.5 cm/s. As buoy speeds increased, so did good RD percentages.

**Table 8. Normalized Speed and Relative Direction statistics for the 0.9 correlation threshold December 01, 1999 to February 29, 2000. (FNMOC data)**

	Total Pairs	Buoy Speed (cm/s)			
Normalized Speed	702	0 - 7.5 490	7.5 - 15.0 164	15.0 - 22.5 40	> 22.5 8
0 - 50%	143(20.4%)	63(12.9%)	62(37.8%)	15(37.5%)	3(37.5%)
50 - 80%	69(9.8%)	40(8.2%)	21(12.8%)	7(17.5%)	1(12.5%)
<b>80 - 120%</b>	<b>98(14.0%)</b>	<b>52(10.6%)</b>	<b>37(22.6%)</b>	<b>7(17.5%)</b>	<b>2(25.0%)</b>
120 - 150%	59(8.4%)	30(6.1%)	23(14.0%)	5(12.5%)	1(12.5%)
150 - 200%	54(7.7%)	44(9.0%)	7(4.3%)	2(5.0%)	1(12.5%)
<b>&gt; 200%</b>	<b>279(39.7%)</b>	<b>261(53.3%)</b>	<b>14(8.5%)</b>	<b>4(10.0%)</b>	<b>0(0.0%)</b>
Relative Direction +/-	702	490	164	40	8
0 - 30°	165(23.5%)	83(16.9%)	63(38.4%)	15(37.5%)	4(50.0%)
30 - 90°	237(33.8%)	170(34.7%)	55(33.5%)	12(30.0%)	0(0.0%)
90 - 180°	300(42.7%)	237(48.4%)	46(28.0%)	13(32.5%)	4(50.0%)

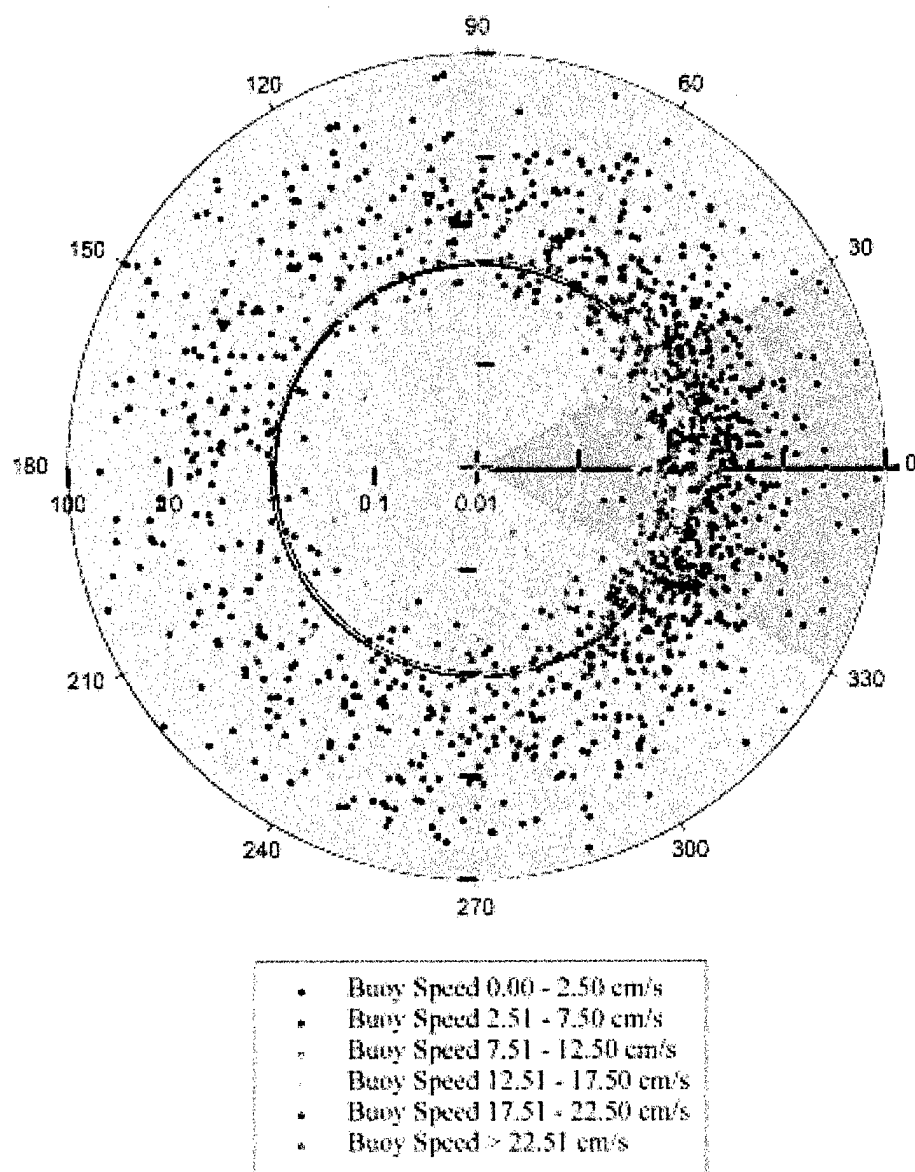
There is a large disparity between NRL and FNMOC statistics when applying the 0.9 correlation threshold. NRL data in Table 5 showed higher percentages than FNMOC. A key statistic is the total number of SSM/I and buoy vector pairs that have a NS value between 80 - 120 %. NRL had a 19.6% NS percentage value between 80 - 120% and FNMOC had a 14.0% NS percentage value between 80 - 120%. The difference in NS

percentages result from compositing differences applied to NRL and FNMOC data. As shown in case study analysis, applying the 0.9 correlation threshold to FNMOC composited data resulted in poor SSM/I and buoy motion vector values. This is also evident in Tables 7 and 8. Poor results are likely attributable to the "drop-in-the-bucket" compositing technique.

Figures 31-34 are polar plots used to visualize normalized SSM/I and buoy motion vectors. The points on the figure indicate the speed and direction of the SSM/I vector relative to the buoy vector. Normalized speed is computed by dividing SSM/I derived speed by buoy speed, with 1.00 indicating buoy speed equal to SSM/I speed. Relative direction was computed by taking the difference between SSM/I and buoy derived directions. A SSM/I vector at  $0^{\circ}$  and 1.0 normalized speed is equal to the buoy vector.

Scaling is standard logarithmic, centered at .01 and ranging to 100. Gray background shading is applied to provide the reader a sense of directional bias and highlight regions of good ( $\pm 30^{\circ}$ ), questionable ( $\pm 30^{\circ} - 90^{\circ}$ ) and bad ( $\pm 90^{\circ} - 180^{\circ}$ ) normalized direction. Buoy speeds are grouped by color every 5 cm/s starting at 0.00 cm/s, with a  $\pm 2.5$  cm/s range.

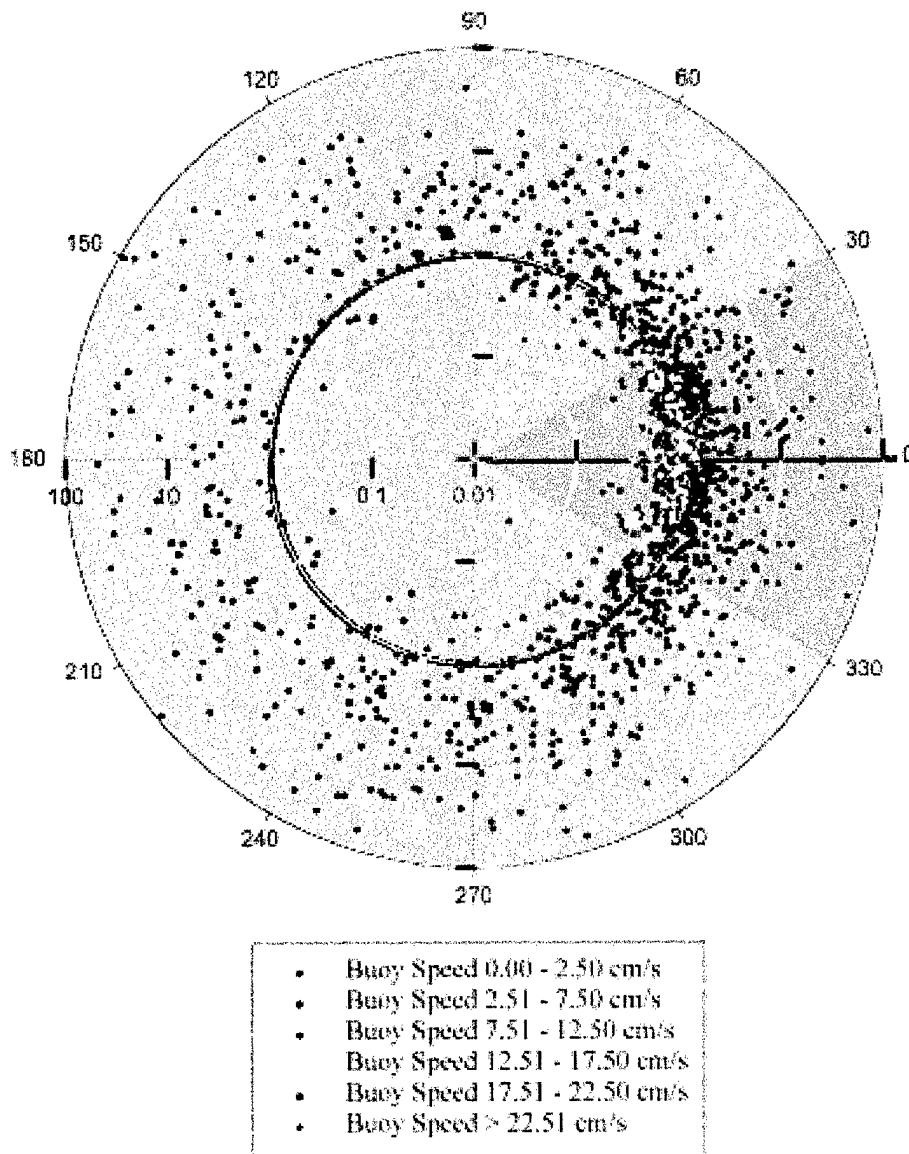
Figure 31 is a Normalized Polar Plot using a 0.7 correlation threshold applied to NRL SSM/I data from December 01<sup>st</sup>, 1999 to February 29<sup>th</sup>, 2000. A clear progression towards a normalized value of speed = 1 and direction = 0° is reflected as buoy speed increases.



**Figure 31.** Polar plot using a 0.7 correlation threshold (NRL data) December 01, 1999 to February 29, 2000.

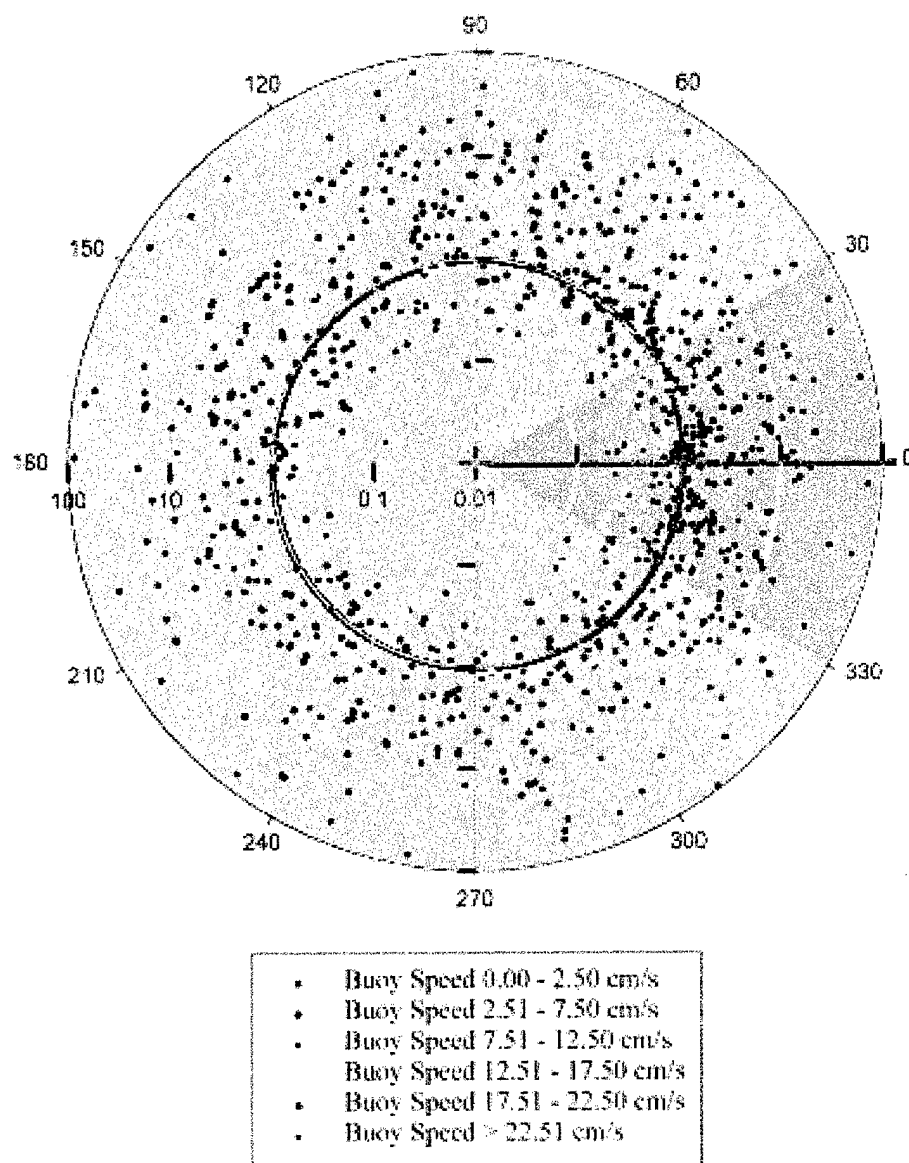


Figure 32 is a Normalized Polar Plot using a 0.9 correlation threshold applied to NRL SSM/I data from December 01<sup>st</sup>, 1999 to February 29<sup>th</sup>, 2000. Progression to normalization as buoy speed increases is clearly depicted with fewer reports plotted in the bad direction range, indicating the removal of bad vector pairs.



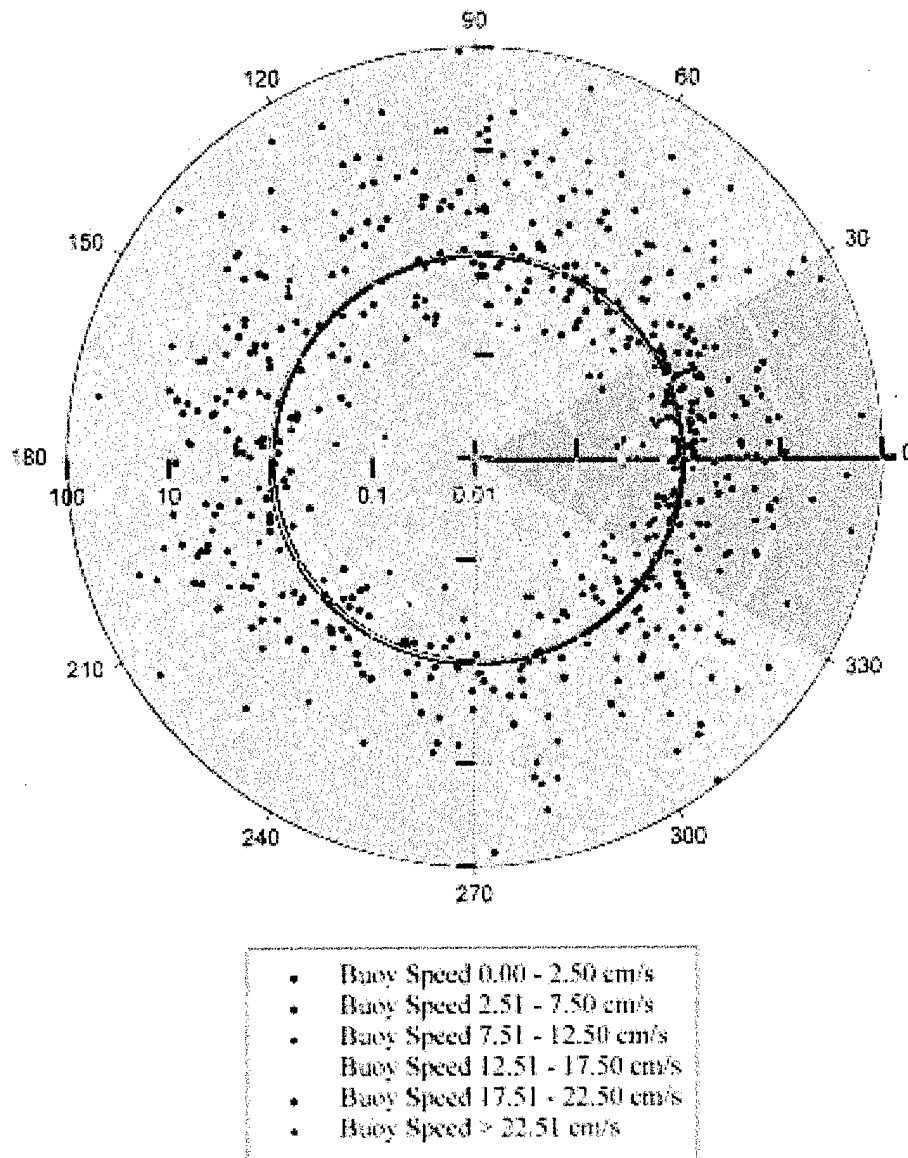
**Figure 32.** Polar plot using a 0.9 correlation threshold (NRL data)  
December 01, 1999 to February 29, 2000.

Figure 33 is a Normalized Polar Plot using a 0.7 correlation threshold applied to FNMOC SSM/I data from February 15<sup>th</sup> to May 30<sup>th</sup>, 2000. A lot of noise is reflected in the plot. A clear progression towards normalization as buoy speed increases is not as evident. Several high buoy speeds are plotted outside the defined good speed and direction range.



**Figure 33.** Polar plot using a 0.7 correlation threshold on (FNMOC data)  
February 15 to May 30, 2000.

Figure 34 is a Normalized Polar Plot using a 0.9 correlation threshold applied to FNMOC SSM/I data from February 15<sup>th</sup> to May 30<sup>th</sup>, 2000. Clear removal of several SSM/I and buoy pairs occur both outside and inside defined good ranges. The plot is very noisy with no clear progression to normalization as buoy speed increases.



**Figure 34.** Polar plot using a 0.9 correlation threshold on (FNMOC data) February 15 to May 30, 2000.

### C. NRL/FNMOC Statistical summary for May 11-14<sup>th</sup>

Case Study 3 for February provided a comparison study between NRL and FNMOC data sets. Unfortunately, low ice motions during that time period prevented a complete analysis for comparing compositing techniques and the effect on the accuracy of ice motions. Ice motions were derived and compared for a three-day period in May using NRL and FNMOC SSM/I data. This time frame was chosen because high ice motions prevail during a period of strong synoptic-scale surface winds.

Tables 9 and 10 contain summary statistics applying a 0.7 correlation threshold for FNMOC and NRL composited data for May 11-14<sup>th</sup>. The total percentage for good pairs (80-120%) of NS is much higher for the NRL data set. NRL ice motions also show a strong tendency for the SSM/I vectors to match the buoy vectors as buoy speed increases. The fraction of good NS values in the FNMOC data set are significantly lower than in the NRL data set. NRL also produces a greater fraction of Relative Direction values in the good range ( $\pm 0-30^\circ$ ) than does the FNMOC data set.

**Table 9. Normalized Speed and Relative Direction statistics for the 0.7 correlation threshold, May 11 - 14<sup>th</sup>, 2000 (FNMOC data).**

	Total Pairs	Buoy Speed (cm/s)			
Normalized Speed	114	0 - 7.5 32	7.5 - 15.0 45	15.0 - 22.5 29	>22.5 8
0 - 50%	29(25.4%)	3(9.4%)	13(28.9%)	10(34.5%)	3(37.5%)
50 - 80%	21(18.4%)	3(9.4%)	10(22.2%)	6(20.7%)	2(25.0%)
<b>80 - 120%</b>	<b>22(19.3%)</b>	<b>4(12.5%)</b>	<b>12(26.7%)</b>	<b>6(20.7%)</b>	<b>0(0.0%)</b>
120 - 150%	9(7.9%)	5(15.6%)	1(2.2%)	1(3.4%)	2(25.0%)
150 - 200%	7(6.1%)	4(12.5%)	2(4.4%)	1(3.4%)	0(0.0%)
<b>&gt; 200%</b>	<b>26(22.8%)</b>	<b>13(40.6%)</b>	<b>7(15.6%)</b>	<b>5(17.2%)</b>	<b>1(12.5%)</b>
Relative Direction +/-	114	32	45	29	8
0 - 30°	37(32.5%)	6(18.8%)	17(37.8%)	10(34.5%)	4(50.0%)
30 - 90°	33(28.9%)	12(37.5%)	11(24.4%)	8(27.6%)	2(25.0%)
90 - 180°	44(38.6%)	14(43.8%)	17(37.8%)	11(37.9%)	2(25%)

**Table 10. Normalized Speed and Relative Direction statistics for the 0.7 correlation threshold, May 11 - 14<sup>th</sup>, 2000 (NRL data).**

	Total Pairs	Buoy Speed (cm/s)			
Normalized Speed	116	0 - 7.5 39	7.5 - 15.0 46	15.0 - 22.5 23	22.5 8
0 - 50%	9(7.8%)	6(15.4%)	3(6.5%)	0(0.0%)	0(0.0%)
50 - 80%	21(18.1%)	7(17.9%)	11(23.9%)	2(8.7%)	1(12.5%)
<b>80 - 120%</b>	<b>33(28.4%)</b>	<b>6(15.4%)</b>	<b>16(34.8%)</b>	<b>6(26.1%)</b>	<b>5(62.5%)</b>
120 - 150%	15(12.9%)	5(12.8%)	4(8.7%)	6(26.1%)	0(0.0%)
150 - 200%	14(12.1%)	7(17.9%)	5(10.9%)	2(8.7%)	0(0.0%)
<b>&gt; 200%</b>	<b>24(20.7%)</b>	<b>8(20.5%)</b>	<b>7(15.2%)</b>	<b>7(30.4%)</b>	<b>2(25.0%)</b>
Relative Direction +/-	116	39	46	23	8
0 - 30°	63(54.3%)	12(30.8%)	30(65.2%)	15(65.2%)	6(75.0%)
30 - 90°	41(35.3%)	19(48.7%)	13(28.3%)	7(30.4%)	2(25.0%)
90 - 180°	12(10.3%)	8(20.5%)	3(6.5%)	1(4.3%)	0(0.0%)

Figures 35 and 36 are Normalized Polar Plots using a 0.7 correlation threshold applied to FNMOC and NRL SSM/I data from May 11-14<sup>th</sup>. A clear progression towards a normalized value of speed equal to 1 and direction equal to 0° is apparent in the NRL plot. FNMOC normalized results are poor in comparison to NRL.

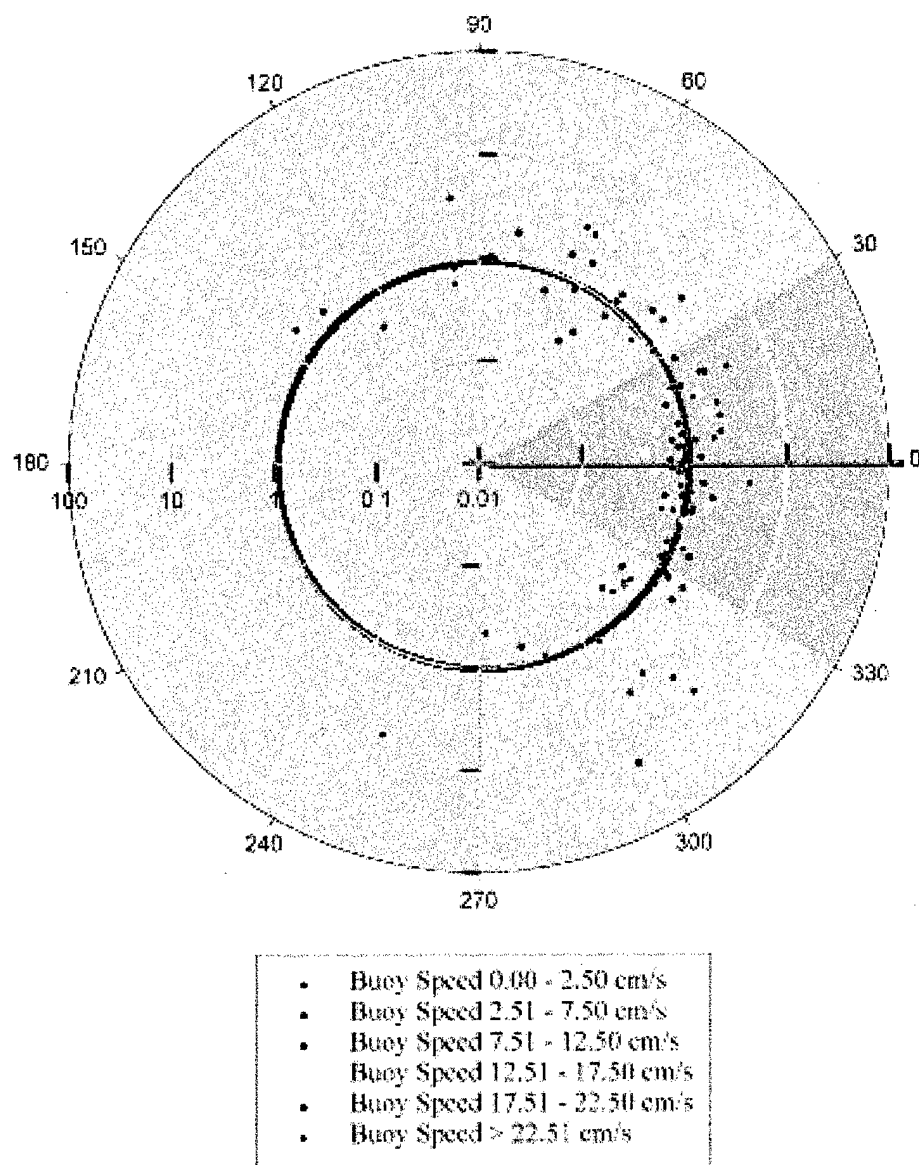


**Figure 35.** NRL Polar plot using a 0.7 correlation threshold  
May 11 - 14<sup>th</sup>, 2000.

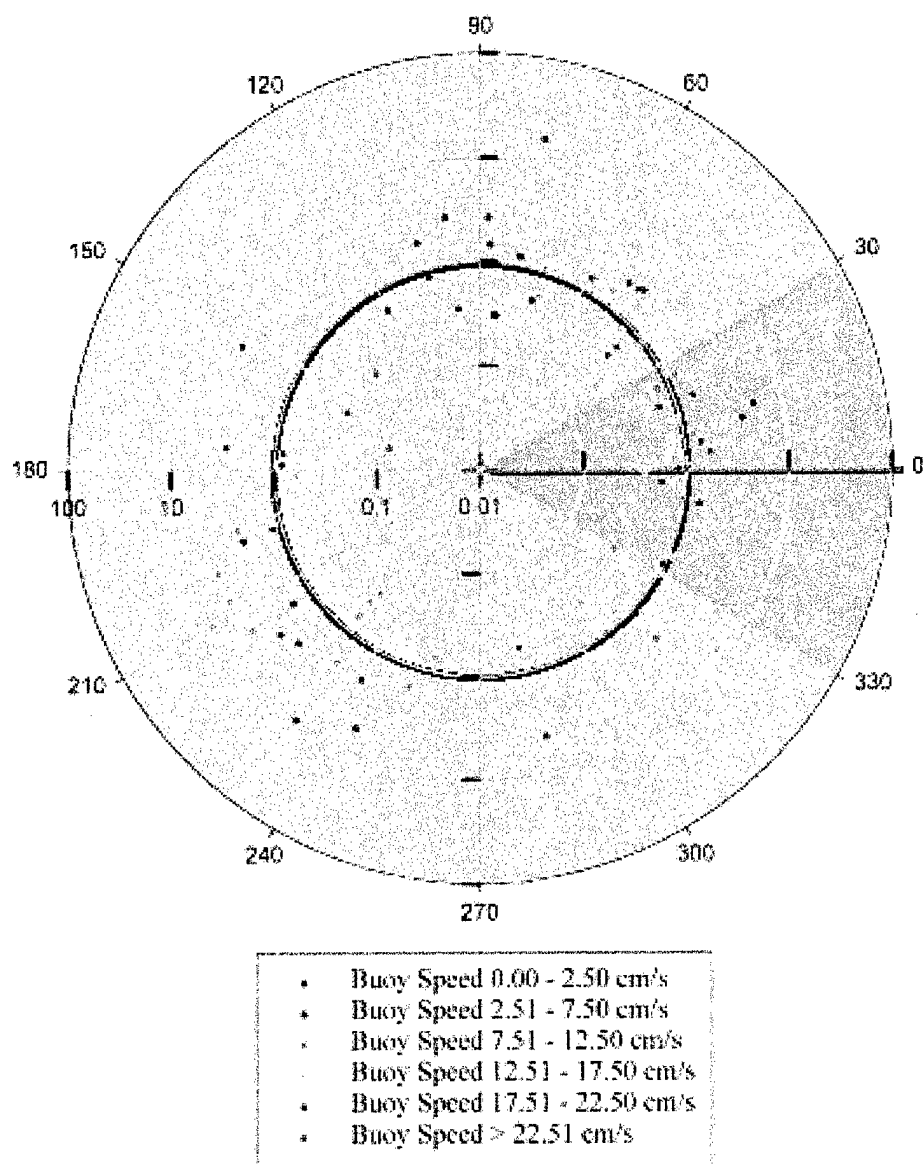


**Figure 36.** FNMOC Polar plot using a 0.7 correlation threshold  
May 11 - 14<sup>th</sup>, 2000.

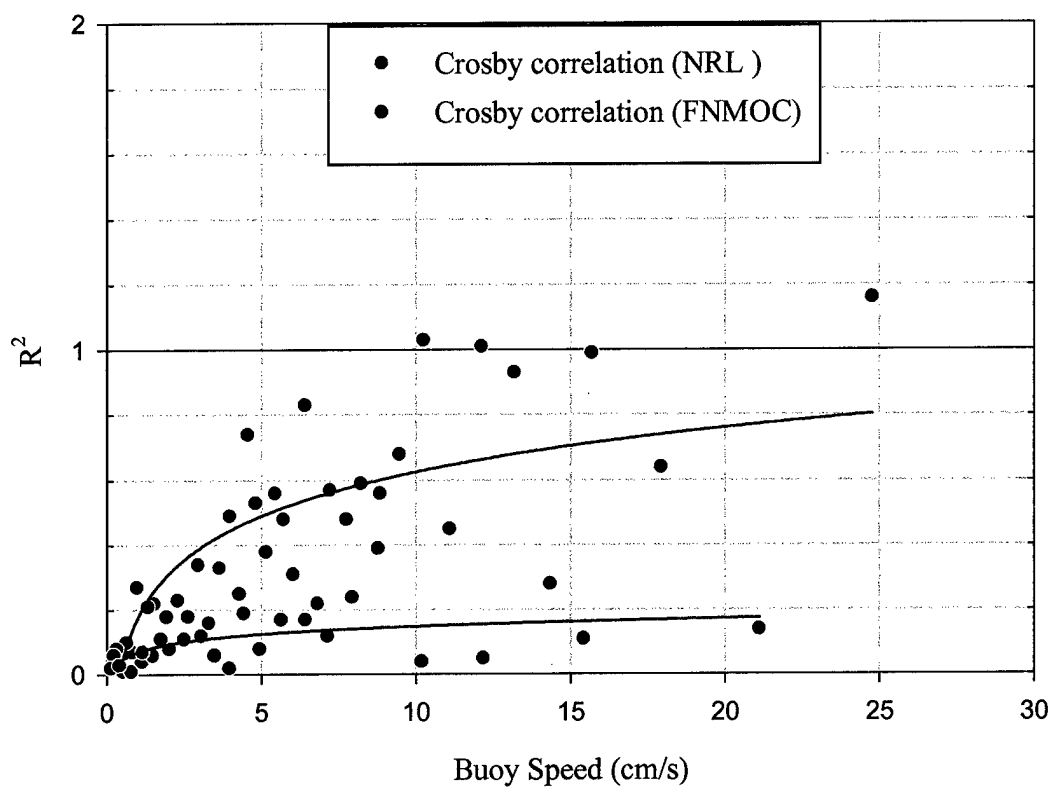
#### D. VECTOR CORRELATION

A vector correlation technique developed by Crosby et al. (1993) was used in this thesis to quantify the quality of SSM/I ice motion vectors. This technique addresses the problem of correlating vector quantities, unique to meteorological and oceanographic studies. Vectors are correlated directly, without decomposition into scalar components. The result is an objective measure of the correlation of two sets of coincident vector pairs.

Code for the Crosby technique was used to compute the square of the vector correlation coefficient ( $R^2$ ). An  $R^2$  value of 2.0 indicates perfect correlation between the vector pairs. Crosby (1993) points out that the sample size must be large enough to include sufficient variation among the vector pairs. Therefore, since the value of  $R^2$  depends slightly on sample size, all calculations below are done with a constant number of vector pairs. To include all information provided by matched pairs and provide a statistically meaningful result, all buoy speeds were collected and sorted starting at 0.00 cm/s. Groups of 25 SSM/I and buoy vector pairs were sequentially entered into Crosby's vector correlation program and plotted in Figures 37 and 38 by their average buoy speed.

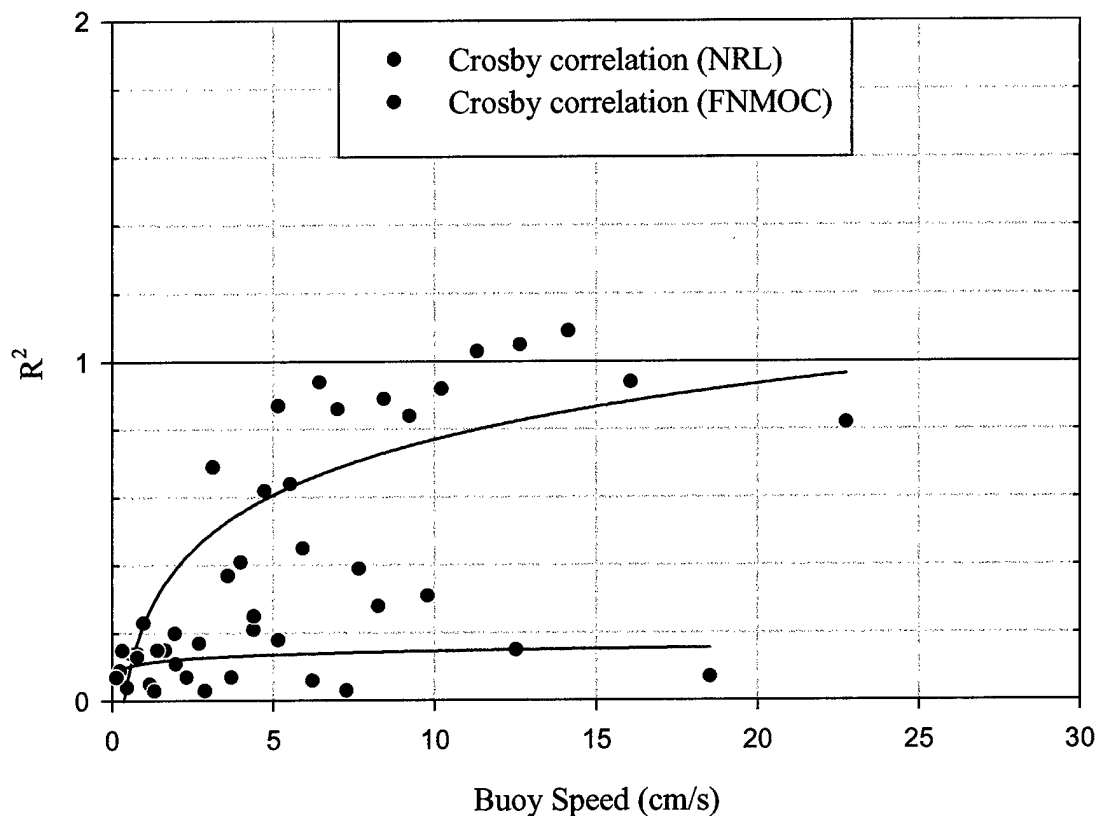


Figure 37 is a vector correlation plot of NRL and FNMOC SSM/I data, applied to SSM/I and buoy motion vector results for the 0.7 correlation threshold. The NRL plot reflects a strong increase in  $R^2$  beginning around 5 cm/s. The FNMOC vectors have consistently low  $R^2$  values at all buoy speeds.



**Figure 37.** Vector correlation coefficient ( $R^2$ ) plot of 0.7 correlated threshold.

Figure 38 is a vector correlation plot of NRL and FNMOC SSM/I data, applied to the 0.9 correlation threshold, SSM/I and buoy motion vector results. The 0.9 correlation threshold clearly reflects a transition of the NRL data similar to that seen in Figure 43. The 0.9 correlation threshold plot for FNMOC is worse than seen in Figure 43 indicating largely uncorrelated vectors.



**Figure 38.** Vector correlation coefficient ( $R^2$ ) plot of 0.9 correlated threshold.

Two conclusions can be made. First, the 0.9 correlation threshold using NRL data provided better results as compared to FNMOC. Most FNMOC data is removed with the 0.9 correlation threshold, leaving a small number of SSM/I and buoy motion vectors to correlate. Second, the oversampling scheme of the ice motion algorithm improves the

resolution of the vector speed calculation. Without over sampling, SSM/I speeds aren't detectable below 7.23 cm/s and Figure 38 clearly indicates correlated values below 7.23 cm/s.

## VI. CONCLUSIONS AND RECOMMENDATIONS

### A. CONCLUSIONS

Meier's adapted 85.5 GHz SSM/I sea ice motion algorithm was applied to SSM/I data received from NRL and FNMOC. Four case studies were subjectively chosen to represent different meteorological conditions and conduct comparisons between NRL and FNMOC. Within the algorithms filtering subroutine, 0.7 and 0.9 correlation thresholds are applied to the SSM/I motion vector field. To assess the quality of the satellite analysis, SSM/I motion vectors were matched with in-situ buoys using two methods: (1) the closest SSM/I vector paired with the buoy motion vector and (2) the median of SSM/I vectors within 5 pixels paired with the buoy motion vector.

Initial study of the algorithm revealed a mapping error contained within the IDL mapper program code. This program converts the geo-reference and mapping Fortran routines into IDL code for adaptation by FNMOC. The code was updated and provided to FNMOC.

As applied to NRL SSM/I data, the 0.7 correlation threshold and median SSM/I to buoy motion vector pairs provided good results. NRL motion vectors correlate well for speeds greater than 4-5 cm/s and correlation increases with higher speeds. A vector correlation coefficient ( $R^2$ ) was computed using a method developed by Crosby et al., (1993). Resulting plots indicate a definitive increase in correlation beginning at about 5 cm/s. The 0.9 correlation threshold does provide slightly increased vector correlation and

a clearer increase in correlation, though a few good SSM/I and buoy motion vector pairs are removed.

When applying the vector correlation to FNMOC SSM/I data, the 0.7 correlation threshold and median SSM/I to buoy motion vector pairs display poor results. The statistical analysis reflects noise and ambiguity, with no distinct increase in correlation as in the NRL vector correlation plot. Vector correlation values are much lower than that of NRL SSM/I data. The 0.9 correlation threshold provided worse results as most good SSM/I and buoy vector pairs were filtered, resulting in yet lower  $R^2$  values. This suggests that the FNMOC compositing produced few motion vectors with pattern correlation greater than 0.7.

Compositing methods appear to be the primary cause of the high statistical differences between NRL and FNMOC SSM/I data. The compositing scheme applied to FNMOC SSM/I data resulted in artificial texture that introduced noise into the motion calculation and produced poor vector correlation with in situ buoys. Compositing NRL SSM/I data in TeraScan produced better ice motion vectors and improved statistical results.

## **B. RECOMMENDATIONS**

The results presented here strongly suggest that the FNMOC compositing use a bi-linear interpolation technique (as used in TeraScan) in the compositing procedure. This will provide the best possible ice motions to the models. A 24-hour or 72-hour motion composite will produce smoother results and display more SSM/I and buoy motion vectors. But care must be given to masking the algorithm's weakness to handle  $T_B$  changes noted during the melt-by-day, freeze-by-night springtime conditions.

The removal of SSM/I vectors greater than  $90^{\circ}$  from wind direction should be considered. Kwok et al., (1998) filters SSM/I derived vectors greater than  $90^{\circ}$  contrary to the gradient wind flow. This can be easily applied, and makes sense when using 1 to 3 day composites. Caution must be exercised as ice motion can lag in response to wind flow or be influenced by a strong wind gradient 100's of kilometers away.

Case studies for this paper were selective and subjective. A real-time extended comparison study using the current algorithm compositing technique and TeraScan composite routine with 0.7 and 0.9-correlation filter for 14/24/72 hour periods should be conducted. Application to a full Arctic seasonal cycle (October - May) using NRL and FNMOC data may provide better insight to the algorithms strengths and weaknesses.

THIS PAGE INTENTIONALLY LEFT BLANK

## LIST OF REFERENCES

Colony, R., and A.S. Thorndike, An Estimate of the Mean Field of Arctic Sea Ice Motion. *J. Geophys. Res.*, 89, 10,623 - 10,629, 1984.

Crosby, D.S., Breaker, L.C., and Gemmil, W.H., A Proposed Definition for Vector Correlation in Geophysics: Theory and Application, *J. Atmos. and Ocean Tech.*, vol. 10, 355-367, 1993.

Emery, W.J., C.W. Fowler, J. Hawkins, and R.H. Preller, Fram Strait Satellite Image-derived Ice Motions, *J. Geophys. Res.*, 96, 22075-22085, 1991.

Emery, W.J., C.W. Fowler, and J.A. Maslanik, Satellite-derived Maps of Arctic and Antarctic Sea Ice Motions: 1988-1994, *Geophys. Res. Letters*, 24, 897-900, 1997.

Fowler, C.W., Ice Motion Derived from Satellite Remote Sensing with Application to Ice Studies in the Beaufort Sea, Ph.D. Dissertation, University of Colorado, 1995.

Kidder, S.Q. and Vonder Haar, T.H., Satellite Meteorology An Introduction, Chapter 3, 1995.

Kwok, R., A. Schweiger, D.A. Rothrock, S. Pang, and C. Kottmeier, Sea Ice Motion from Satellite Passive Microwave Imagery Assessed with ERS SAR and Buoy Motions, *J. Geophys. Res.*, 103(C4), 8191-8214, 1998.

Meier, W. N., Implementation of the University of Colorado Ice Motion-tracking Algorithm using SSM/I 85 GHz Imagery from Fleet Numerical Meteorological and Oceanographic Center, *Technical Manual*, 1999.

Meier, W. N., Application of Data Assimilation Methods for Analysis and Integration of Observed and Modeled Arctic Sea Ice Motions, Ph.D. Dissertation, University of Colorado, Boulder, 212 pp. 1998.

National Snow and Ice Data Center, Sea Ice Concentrations from Nimbus-7 SMMR and DMSP SSM/I Passive Microwave Data, June 1997, ([http://nsdic.org/NASA/GUIDE/docs/dataset\\_documents/gsfctime\\_series\\_dataset\\_document.html](http://nsdic.org/NASA/GUIDE/docs/dataset_documents/gsfctime_series_dataset_document.html)).

National Snow and Ice Data Center, DMSP SSM/I Daily Polar Gridded Brightness Temperatures, third revised edition, 1997, ([http://nsdic.org/NASA/GUIDE/docs/dataset\\_documents/dmsp\\_ssmi\\_brightness\\_temperatures.html](http://nsdic.org/NASA/GUIDE/docs/dataset_documents/dmsp_ssmi_brightness_temperatures.html)).

Physical Oceanography Distributed Active Archive Center, NASA Jet Propulsion Laboratory, April 2000, ([http://podaac.jpl.nasa.gov:2031/SENSOR\\_DOCS/ssmi.html](http://podaac.jpl.nasa.gov:2031/SENSOR_DOCS/ssmi.html)).



Polar Science Center, International Arctic Buoy Programme, Applied Physics  
Laboratory, University of Washington, revised February 1996,  
(<http://iabp.apl.washington.edu>).

## INITIAL LIST

1. Defense Technical Information Center .....2  
8725 John J. Kingman Road, Suite 0944  
Ft. Belvoir, VA 22060-6218
  
2. Dudley Knox Library .....2  
Naval Postgraduate School  
411 Dyer Road  
Monterey, CA 93943-5101
  
3. Dr. Walt Meier .....1  
National/Naval Ice Center  
Federal Building #4  
4251 Suitland Road  
Washington, DC 20395
  
4. Commanding Officer .....1  
FLENUMMETOCCEN  
7 Grace Hopper Ave, Stop 1  
Monterey, CA 93943-5501
  
5. Naval Research Lab .....1  
7 Grace Hopper Ave, Stop 1  
Monterey, CA 93943
  
6. Chairman .....1  
Department of Meteorology  
Naval Postgraduate School  
Monterey, CA 93943-5000
  
7. Chairman .....1  
Department of Oceanography  
Naval Postgraduate School  
Monterey, CA 93943-5000
  
8. Professor Philip A. Durkee, MR/De .....2  
Naval Postgraduate School  
Monterey, CA 93943-5000
  
9. Dr. Jeffrey L. Haferman .....1  
FLENUMMETOCCEN  
7 Grace Hopper Ave, Stop 1  
Monterey, CA 93943-5501

10. LCDR Dave Carsten .....	2
#8 Micmac Lane	
Brunswick, ME 04011	